

Instrumental and Proximal Causal Inference with Gaussian Processes

Yuqi Zhang¹, Krikamol Muandet², Dino Sejdinovic³,
Edwin Fong¹, and Siu Lun Chau⁴

¹Department of Statistics and Actuarial Science, University of Hong Kong, Hong Kong
²Rational Intelligence Lab, CISA Helmholtz Center for Information Security, Germany
³Australian Institute for Machine Learning, The University of Adelaide, Australia
⁴Epistemic Intelligence & Computation Lab, College of Computing & Data Science,
Nanyang Technological University, Singapore

March 3, 2026

Abstract

Instrumental variable (IV) and proximal causal learning (Proxy) methods are central frameworks for causal inference in the presence of unobserved confounding. Despite substantial methodological advances, existing approaches rarely provide reliable epistemic uncertainty (EU) quantification. We address this gap through a Deconditional Gaussian Process (DGP) framework for uncertainty-aware causal learning. Our formulation recovers popular kernel estimators as the posterior mean, ensuring predictive precision, while the posterior variance yields principled and well-calibrated EU. Moreover, the probabilistic structure enables systematic model selection via marginal log-likelihood optimization. Empirical results demonstrate strong predictive performance alongside informative EU quantification, evaluated via empirical coverage frequencies and decision-aware accuracy–rejection curves. Together, our approach provides a unified, practical solution for causal inference under unobserved confounding with reliable uncertainty.

Keywords: Gaussian processes, Causal Inference, Uncertainty Quantification

1 Introduction

Estimating causal effects from observational data is central to decision-making across a wide range of disciplines. A major challenge, however, is the presence of unobserved confounders, which can bias standard estimators and compromise causal validity. Among the frameworks that address this issue, Instrumental Variables (IV) [Angrist and Krueger, 1992, Stock and Trebbi, 2003] and Proximal Causal Learning (Proxy) [Kuroki and Pearl, 2014, Tchetgen et al., 2020, Miao et al., 2024] have emerged as foundational tools. Under suitable structural assumptions, both frameworks enable the identification of causal effects despite unobserved

confounding, that is, they construct valid estimators from observational data for reasoning about causal estimands.

Recent advances in machine learning have provided a rich class of such estimators, ranging from kernel-based methods [Singh et al., 2019, Muandet et al., 2020, Mastouri et al., 2021] to deep learning approaches [Xu et al., 2020]. While these estimators have demonstrated strong empirical performance and have been studied extensively from a theoretical perspective [Chen et al., 2025], they primarily focus on point estimation of causal effects. As a result, principled predictive uncertainty quantification (UQ)—capturing how confident a model is in its causal estimates—remains comparatively underdeveloped. We argue that modelling predictive uncertainty is nevertheless also a crucial component for reliable causal inference.

Informative predictive uncertainty is crucial for several reasons. First, it is essential for trustworthy and responsible deployment [Vashney, 2022], particularly in safety-critical settings where causal estimates inform real-world interventions. Second, predictive uncertainty enables risk-aware decision-making, including conservative and selective deployment [Cortes et al., 2016, Shaker and Hüllermeier, 2020], or deferral [Madras et al., 2018] when available evidence is insufficient. Third, predictive uncertainty plays a central role in downstream tasks such as causal data fusion [Chau et al., 2021b], causal active learning [Gao and Sejdinovic, 2025], and finding optimal treatment [Aglietti et al., 2020], where it governs how evidence is weighted and how limited resources are allocated. These considerations become even more critical—and substantially more challenging—in the presence of unobserved confounding, where uncertainty must reflect not only data variability but also incomplete knowledge of the confounders.

Despite its importance, existing approaches to quantifying predictive uncertainty in causal inference with unobserved confounding remain limited. Model-agnostic UQ strategies are typically bootstrap-based and heuristic, and therefore lack a coherent probabilistic interpretation; the uncertainty they quantify often reflects sensitivity to the resampling procedure rather than genuine model confidence. Bayesian approaches offer a more principled alternative, but frequently incur substantial computational and methodological overhead, impose strong parametric assumptions [Lopes and Polson, 2014], or rely on artificial data-generating mechanisms [Wang et al., 2021]. Moreover, evaluations of uncertainty quality are often restricted to basic coverage-based metrics [Hu et al., 2023], rather than assessing how effectively uncertainty estimates support downstream decision-making—a perspective that has received increasing attention in the broader uncertainty quantification literature [Shaker and Hüllermeier, 2020, Chau et al., 2026].

Contributions. We propose a Gaussian process (GP) [Rasmussen, 2003] framework with principled uncertainty quantification for both the IV and Proxy settings. Building on the observation that learning the unconfounded structural function in both settings reduces to solving a Fredholm integral equation, we leverage the theory of deconditional kernel embeddings [Hsu and Ramos, 2019a], which act as pseudo-inverses of conditional expectation operators, and adapt their GP formulation [Chau et al., 2021a] to causal learning under unobserved confounding. The resulting methods, **GPIV** and **GProxy**, form a unified Bayesian nonparametric framework for causal estimation across both settings.

For estimation, we show that the posterior means of **GPIV** and **GPProxy** recover the frequentist estimators underlying widely used kernel-based approaches such as Kernel IV (KIV; Singh et al. [2019]) and Kernel Negative Control (KNC; Singh [2023]). Consequently, our approach inherits their strong modeling performance and established asymptotic guarantees, while the Bayesian formulation additionally equips them with principled predictive uncertainty quantification. As an added benefit, our Bayesian framework naturally supports principled model selection via marginal likelihood optimization, yielding strong empirical performance without reliance on ad hoc parameter initialization or extensive cross-validation (CV) commonly used in frequentist approaches.

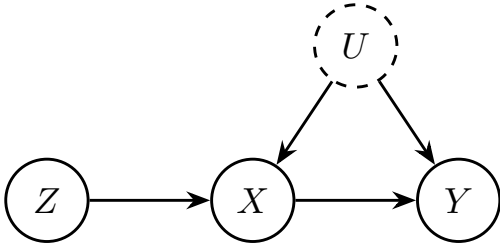
Our empirical results demonstrate consistently strong predictive performance compared to state-of-the-art baselines, which we attribute to the holistic model selection enabled by our Bayesian formulation. To evaluate the quality of the quantified predictive uncertainty, we begin by reporting empirical coverage frequencies, followed by assessing the informativeness of the uncertainty in downstream decision-making tasks, such as selective inference, where we evaluate how effectively uncertainty estimates identify instances for which predictions should be withheld by extending the evaluation framework of Shaker and Hüllermeier [2020].

The remainder of the paper is organized as follows. Section 2 introduces the IV and Proxy setting, together with the necessary background on kernel methods and GPs. Section 3 presents our technical contributions. Section 4 reviews related work. Section 5 provides results of experiments and simulations, and Section 6 concludes the paper.

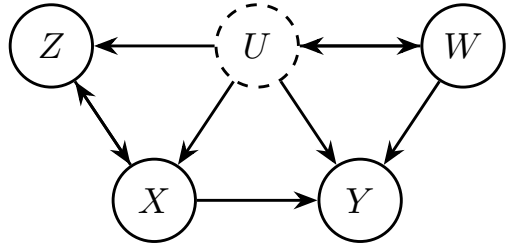
2 Preliminary

Notations. Let \mathcal{X} , \mathcal{Y} , \mathcal{U} , and \mathcal{Z} denote the spaces of the treatment, outcome, (unobserved) confounder, and instrument, respectively. Uppercase letters X , Y , U , and Z denote random variables taking values in \mathcal{X} , \mathcal{Y} , \mathcal{U} , and \mathcal{Z} , with corresponding distributions P_X , P_Y , P_U and P_Z . Lowercase letters denote their realisations. In the Proxy setting, Z instead denotes the treatment proxy, and an additional variable $W \in \mathcal{W}$, serves as the outcome proxy.

Let $\mathcal{H}_{\mathcal{X}}$ denote the reproducing kernel Hilbert space (RKHS) [Aronszajn, 1950] for functions on \mathcal{X} associated with the kernel $k_{\mathcal{X}} : \mathcal{X} \times \mathcal{X} \rightarrow \mathbb{R}$. With an abuse of notation, we define $k_x = k_{\mathcal{X}}(x, \cdot)$ as the canonical feature map for $x \in \mathcal{X}$, and $k_X = k_{\mathcal{X}}(X, \cdot)$ as the induced random elements in $\mathcal{H}_{\mathcal{X}}$ map by the random variable X . For simplicity, we denote $k_{x,x'}$ as $k_{\mathcal{X}}(x, x')$ for two test points. Given realizations $\mathbf{x} = (x_1, \dots, x_n)^\top$, we define kernel matrices by stacking the kernel elements maps along columns as $\Psi_{\mathbf{x}} = [k_{x_1}, \dots, k_{x_n}]$ and the Gram matrix as $\mathbf{K}_{\mathbf{xx}} = \Psi_{\mathbf{x}}^\top \Psi_{\mathbf{x}} = [k_{x_i, x_j}]_{1 \leq i, j \leq n}$. For a given test point x' , we write $\mathbf{K}_{x'\mathbf{x}} = [k_{x', x_1}, \dots, k_{x', x_n}]$ as the evaluation vector. RKHSs, kernels, and matrices associated with variables Z, W are defined analogously.



(a) DAG for IV



(b) DAG for Proxy

Figure 1: Causal Graphs

2.1 Instrumental Variable

In the IV regression problem, the goal is to estimate a structural function $f : \mathcal{X} \rightarrow \mathcal{Y}$ under the following structural equation model, also illustrated in Figure 1a:

$$Y = f(X) + U, \quad \mathbb{E}[U] = 0, \quad \mathbb{E}[U | X] \neq 0, \quad (1)$$

where U is a unobserved, mean-zero confounder that influences both the treatment X and outcome Y . The presence of this confounding renders direct estimation via standard regression methods invalid, since the conditional expectation $\mathbb{E}[Y | X = x]$ no longer coincides with the structural function $f(x)$. Under Pearl’s do-calculus framework [Pearl, 2009], the structural function corresponds to the average treatment effect (ATE)

$$f(x) = \mathbb{E}[Y | do(X = x)].$$

To address unobserved confounding, an IV Z can be introduced to enable identification of the structural function f . The key requirement is that the instrument is exogenous with respect to the unobserved confounder, in the sense that $\mathbb{E}[U | Z] = 0$; formal conditions are presented in Appendix A. Taking conditional expectations with respect to Z on both sides of Equation 1 yields

$$\mathbb{E}[Y | Z] = \mathbb{E}[f(X) | Z] = \int_{\mathcal{X}} f(X) dP(X | Z), \quad (2)$$

which defines a Fredholm integral equation of the first kind. A variety of approaches have been proposed to solve this ill-posed inverse problem. For example, Muandet et al. [2019] formulated this as a convex-concave saddle-point problem. In this work, we instead adopt a deconditioning [Hsu and Ramos, 2019b] perspective, which constructs a pseudo-inverse of the conditional expectation operator to recover f . Specifically, we build on the GP deconditional formulations of Chau et al. [2021a], which we adapt to the IV setting and describe in detail in Section 3.

2.2 Proximal Causal Learning

Compared with the IV setting, the assumptions in the proxy are further relaxed. Instead of assuming the existence of an IV that has no unobserved common cause with the outcome,

informally, we assume the treatment proxy Z and the outcome proxy W provide sufficient information about the unobserved confounder U , as Figure 1b shows.

Our goal remains the estimation of the ATE $\mathbb{E}[Y \mid \text{do}(X = x)]$, which is again different with the conditional mean $\mathbb{E}[Y \mid X = x]$ due to the presence of U . Under the assumptions in the Appendix A, following the results of Miao et al. [2018, 2024], we first solve for a bridge function h satisfying the Fredholm integral equation:

$$\mathbb{E}[Y \mid X, Z] = \int_{\mathcal{W}} h(X, W) dP(W \mid X, Z). \quad (3)$$

Finally, we marginalize over W to identify the ATE:

$$f(x) = \mathbb{E}[Y \mid \text{do}(X = x)] = \int_{\mathcal{W}} h(x, W) dP(W) \quad (4)$$

We note that Mastouri et al. [2021], Singh [2023] also proposed kernel-based approaches to tackle proxy through solving the Fredholm integral equation, similar to IV. We adopt a similar strategy but provide a Bayesian perspective, leveraging the deconditioning GP to recover the ATE from eq.3.

2.3 Kernel embeddings of distributions

Kernel mean embeddings (KME). KME [Smola et al., 2007, Muandet et al., 2016] provides a flexible framework for representing and manipulating probability distributions without requiring parametric assumptions. In particular, the KME for P_X is defined as $\mu_X = \mathbb{E}[k(X, \cdot)] \in \mathcal{H}_X$, which can be empirically estimated by

$$\hat{\mu}_X = \frac{1}{n} \sum_{i=1}^n k_{x_i}.$$

For a broad class of *characteristic* kernels, such as the Gaussian and Matérn kernels on \mathbb{R}^d , this mapping is injective.

Besides computing the kernel mean, higher-order moments of the induced random element maps can be utilized to model relationships between variables. In particular, the (cross-)covariance operator between variables X, Z is defined as

$$C_{XZ} = \mathbb{E}[k_X(X, \cdot) \otimes k_Z(Z, \cdot)] \in \mathcal{H}_X \otimes \mathcal{H}_Z,$$

which can also be estimated via empirical averages, i.e.

$$\hat{C}_{XZ} = \frac{1}{n} \sum_{i=1}^n k_{x_i} \otimes k_{z_i} = \frac{1}{n} \Psi_X \Psi_Z^\top.$$

Similarly, the covariance (or variance) operator C_{XX} and its empirical estimator \hat{C}_{XX} are defined analogously.

Conditional mean embeddings (CME). Conditional distributions $P_{X|Z}$ can also be embedded in the RKHS as $\mu_{X|Z=z} = \mathbb{E}[k_X | Z = z] \in \mathcal{H}_{\mathcal{X}}$. However, as we often observe samples of X, Z jointly, the standard Monte Carlo estimator for CME is not desirable. Instead, following [Song et al. \[2009\]](#), it is more common to associate the CME with the conditional mean operator (CMO) $C_{X|Z} : \mathcal{H}_{\mathcal{Z}} \rightarrow \mathcal{H}_{\mathcal{X}}$, which satisfies $C_{X|Z}k_z = \mu_{X|Z=z}$ for all $z \in \mathcal{Z}$.

Regularity assumptions on the conditional distribution (see [Klebanov et al. \[2020\]](#) for a rigorous treatment) ensure that the CMO is a well-defined bounded operator which admits the representation $C_{X|Z} = C_{XZ}C_{ZZ}^\dagger$, where \dagger denotes the Moore-Penrose pseudoinverse. A standard estimator of CMO is given by [Song et al. \[2013\]](#) as

$$\hat{C}_{X|Z} = \Psi_{\mathbf{x}}(\mathbf{K}_{\mathbf{zz}} + \eta I)^{-1} \Psi_{\mathbf{z}}^\top, \quad (5)$$

which includes a Tikhonov regularization term $\eta > 0$. The empirical CME is then

$$\hat{\mu}_{X|Z=z} = \hat{C}_{X|Z}k_z$$

for any $z \in \mathcal{Z}$.

Deconditional mean embeddings (DME). DME [\[Hsu and Ramos, 2019a\]](#) serve as natural counterparts to CME. In CME, we have

$$\langle \mu_{X|Z=z}, f \rangle_{\mathcal{H}_{\mathcal{X}}} = \mathbb{E}[f(X) | Z = z]$$

for all $f \in \mathcal{H}_{\mathcal{X}}$. DME, denoted $\mu_{X=x|Z} \in \mathcal{H}_{\mathcal{Z}}$, reverses this process: it recovers the function from the conditional mean via the relation

$$\langle \mu_{X=x|Z}, \mathbb{E}[f(X) | Z = \cdot] \rangle_{\mathcal{H}_{\mathcal{Z}}} = f(x).$$

Analogous to the relationship between the CMO and CME, the deconditional mean operator (DMO) $D_{X|Z} : \mathcal{H}_{\mathcal{X}} \rightarrow \mathcal{H}_{\mathcal{Z}}$ is associated with DME through the identity $\mu_{X=x|Z} = D_{X|Z}k_x$ for all $x \in \mathcal{X}$. This operator acts as a pseudoinverse of CMO, satisfying

$$(D_{X|Z})^\top \mathbb{E}[f(X) | Z = \cdot] = f$$

for all $f \in \mathcal{H}_{\mathcal{X}}$. Under regularity assumptions [\[Hsu and Ramos, 2019a\]](#), the DMO can be expressed as a composition of cross-covariance operators and CMOs:

$$D_{X|Z} = (C_{X|Z}C_{ZZ})^\top (C_{X|Z}C_{ZZ}(C_{X|Z})^\top)^{-1}.$$

DMO offers an alternative way to derive frequentist estimators for the ATE by recovering the true functions from the Fredholm integral equations (eqs. [2](#), [3](#)). This yields two estimators, which we name DIV and DProxy (detailed in [Appendix B](#)); however, they do not provide uncertainty quantification.

3 Methods: Deconditional GP for IV and Proxy

In this section, we adopt the deconditioning Gaussian process framework, building on [Chau et al. \[2021a\]](#). That work introduced a Bayesian model whose posterior means recover frequentist DMO-based estimators in statistical downscaling (a connection unrelated to causal inference).¹ We demonstrate how this model can be adapted to instrumental variable (IV) and proxy settings, allowing us to recover the structural function f from Eqs.2–4 while simultaneously enabling predictive uncertainty quantification. Proofs, technical assumptions, and detailed derivations are deferred to Appendix C.

3.1 GP models for IV

We place a GP prior $\mathcal{GP}(0, k)$ on f , where k is a kernel defined on \mathcal{X} . Given observations $\mathcal{D} = (\mathbf{x}, \mathbf{y}, \mathbf{z})$, we aim to derive the posterior distribution of f conditioned on \mathcal{D} . To this end, we consider the following additive noise model:

$$\mathbf{y} \mid \mathbf{z} \sim \mathcal{N}(g(\mathbf{z}), \sigma^2 I), \quad g(z) = \mathbb{E}_X[f(X) \mid Z = z]. \quad (6)$$

We begin with a result on conditional mean processes from [Chau et al. \[2021a\]](#), which ensures the joint Gaussianity of $f(\mathbf{x})$ and \mathbf{y} given \mathcal{D} , and adapt it to our IV setting:

Proposition 3.1. *(CMP for IV.) Under assumptions C.1, C.2, the conditional mean process $\{g(z), z \in \mathcal{Z}\}$ induced by f with respect to $P_{X|Z}$ defined as:*

$$g(z) = \mathbb{E}_X[f(X) \mid Z = z] = \int f(X) dP(X \mid Z = z)$$

is a Gaussian Process $g \sim \mathcal{GP}(0, q)$, with covariance kernel

$$q(z, z') = \text{cov}(g(z), g(z')) = \langle \mu_{X|Z=z}, \mu_{X|Z=z'} \rangle_{\mathcal{H}_X}, \quad (7)$$

where $\mu_{X|Z=z}$ is the CME of $P_{X|Z=z}$ in the RKHS \mathcal{H}_X .

Proposition 3.1 implies the joint distribution is Gaussian:

$$\begin{bmatrix} f(\mathbf{x}) \\ \mathbf{y} \end{bmatrix} \sim \mathcal{N}\left(\begin{bmatrix} 0 \\ 0 \end{bmatrix}, \begin{bmatrix} \mathbf{M}_1 & \mathbf{M}_2 \\ \mathbf{M}_2^\top & \mathbf{M}_3 \end{bmatrix}\right). \quad (8)$$

We now examine further the covariance matrices, with derivations provided in the Appendix C. From the GP prior, note that $\text{cov}(f(x), f(x')) = k_{x,x'}$, which gives

$$\mathbf{M}_1 = \text{cov}(f(\mathbf{x}), f(\mathbf{x})) = \mathbf{K}_{\mathbf{xx}}.$$

Similarly, based on the kernel for g in (eq 7), we define

$$\mathbf{Q}_{\mathbf{zz}} = \text{cov}(g(\mathbf{z}), g(\mathbf{z})) = (C_{X|Z}\Psi_{\mathbf{z}})^\top C_{X|Z}\Psi_{\mathbf{z}}$$

¹The term “deconditioning GP” reflects this correspondence; however, neither [Chau et al. \[2021a\]](#) nor the present framework relies directly on DMOs.

as the kernel matrix induced by q on \mathbf{z} . Consequently,

$$\mathbf{M}_3 = \mathbf{Q}_{\mathbf{zz}} + \sigma^2 I.$$

For \mathbf{M}_2 , the covariance $\text{cov}(f(x), y) = \text{cov}(f(x), g(z))$ is expressed as an inner product of features: $\langle k_x, \mu_{X|Z=z} \rangle_{\mathcal{H}_X}$. This leads to

$$\mathbf{M}_2 = \text{cov}(f(\mathbf{x}), \mathbf{y}) = \Psi_{\mathbf{x}}^\top C_{X|Z} \Psi_{\mathbf{z}}.$$

Finally, using Gaussian conditioning, we obtain:

Proposition 3.2. *Let $\tilde{\mathbf{Q}} = \mathbf{Q}_{\mathbf{zz}} + \sigma^2 I$. The posterior $f \mid \mathbf{y}$ given data $(\mathbf{x}, \mathbf{y}, \mathbf{z})$ is a GP with mean μ and covariance κ :*

$$\begin{aligned} \mu(x) &= k_x^\top C_{X|Z} \Psi_{\mathbf{z}} \tilde{\mathbf{Q}}^{-1} \mathbf{y}, \\ \kappa(x, x') &= k_{x,x'} - k_x^\top C_{X|Z} \Psi_{\mathbf{z}} \tilde{\mathbf{Q}}^{-1} \Psi_{\mathbf{z}}^\top C_{X|Z}^\top k_{x'}. \end{aligned}$$

To obtain a finite data estimate of the mean and covariance, we need to first estimate the CMO/CME, which corresponds to the usual first stage regression in the KIV ([Singh et al., 2019]), after that we can replace $C_{X|Z}$ with

$$\hat{C}_{X|Z} := \Psi_{\mathbf{x}} (\mathbf{L}_{\mathbf{zz}} + \eta I)^{-1} \Psi_{\mathbf{z}}^\top$$

and $\mathbf{Q}_{\mathbf{zz}}$ with

$$\hat{\mathbf{Q}}_{\mathbf{zz}} = (\hat{C}_{X|Z} \Psi_{\mathbf{z}})^\top \hat{C}_{X|Z} \Psi_{\mathbf{z}}.$$

Therefore, we obtain our empirical estimators for the posterior mean and covariance of the structure function f :

$$\begin{aligned} \hat{\mu}(x) &= \mathbf{K}_{x\mathbf{x}} \mathbf{A} (\mathbf{A}^\top \mathbf{K}_{\mathbf{xx}} \mathbf{A} + \sigma^2 I)^{-1} \mathbf{y}, \\ \hat{\kappa}(x, x') &= k_{x,x'} - \mathbf{K}_{x\mathbf{x}} \mathbf{A} (\mathbf{A}^\top \mathbf{K}_{\mathbf{xx}} \mathbf{A} + \sigma^2 I)^{-1} \mathbf{A}^\top \mathbf{K}_{\mathbf{x}x'} \end{aligned}$$

where $\mathbf{A} = (\mathbf{K}_{\mathbf{zz}} + \eta I)^{-1} \mathbf{K}_{\mathbf{zz}}$ is the mediation matrix.

Both our operator-based deconditioning approach (DIV) and the posterior mean of GP formulation (GPIV) yield closed-form estimators, with the relationship specified by the following proposition.

Proposition 3.3. *(Equivalency between KIV, DIV, and GPIV.) Assume $\mathbf{K}_{\mathbf{xx}}$, $(\mathbf{A}^\top \mathbf{K}_{\mathbf{xx}} \mathbf{A} + \sigma^2 I)$ are invertible, the estimator of KIV, DIV, and the mean posterior of GPIV are equivalent.*

3.2 GP models for Proxy

As in GPIV, we construct a GP model for $f(x)$ and derive its posterior given the observed data $\mathcal{D} = (\mathbf{x}, \mathbf{y}, \mathbf{z}, \mathbf{w})$. We begin by placing a GP prior $\mathcal{GP}(0, k)$ on the bridge function h , where $k = k_X \cdot k_W$ on the product space $\mathcal{X} \times \mathcal{W}$. Adopting an additive noise model analogous to (eq 6) in the IV setting, we assume

$$\mathbf{y} \mid \mathbf{x}, \mathbf{z} \sim \mathcal{N}(g(\mathbf{x}, \mathbf{z}), \sigma^2 I), \text{ where } g(x, z) = \mathbb{E}_W [h(x, W) \mid X = x, Z = z].$$

We obtain a conditional mean process result similar to that in the previous section.

Proposition 3.4. (Conditional Mean Process for Proxy Settings.) Let $g(x, z) : x \in \mathcal{X}, z \in \mathcal{Z}$ be the conditional mean process induced by the bridge function h , defined as

$$g(x, z) = \int_{\mathcal{W}} h(x, W) dP(W|X = x, Z = z).$$

Then, under standard regularity assumptions (C.5, C.6) and by linearity, g follows a GP $g \sim \mathcal{GP}(0, q)$ with covariance kernel

$$q((x, z), (x', z')) = \text{cov}(g(x, z), g(x', z')) = k_{x, x'} \langle \mu_{W|X=x, Z=z}, \mu_{W|X=x', Z=z'} \rangle_{\mathcal{H}_W}. \quad (9)$$

Our primary interest lies in recovering the structural function f appearing in equation (eq 4), which requires marginalizing the outcome proxy W from the bridge function h . By linearity, f itself will also be a GP:

Proposition 3.5. Define $f(x) = \int h(x, W) dP(W)$. Under mild regularity assumption C.8, f is almost surely a GP $f \sim \mathcal{GP}(0, r)$ with covariance kernel

$$r(x, x') = \text{cov}(f(x), f(x')) = k_{x, x'} \|\mu_W\|_{\mathcal{H}_W}^2. \quad (10)$$

Consequently, in the proxy setting we obtain the following joint Gaussian distribution:

$$\begin{bmatrix} f(\mathbf{x}) \\ \mathbf{y} \end{bmatrix} \sim \mathcal{N} \left(\begin{bmatrix} 0 \\ 0 \end{bmatrix}, \begin{bmatrix} \mathbf{L}_1 & \mathbf{L}_2 \\ \mathbf{L}_2^\top & \mathbf{L}_3 \end{bmatrix} \right). \quad (11)$$

Based on the covariance kernel specified in (eq 10), we obtain $\mathbf{L}_1 = \text{cov}(f(\mathbf{x}), f(\mathbf{x})) = c_W \mathbf{K}_{\mathbf{xx}}$, where $c_W = \|\mu_W\|_{\mathcal{H}_W}^2$.

The matrix \mathbf{L}_3 consists of two components. The first component originates from the covariance kernel q defined in (eq 9), given by

$$\mathbf{Q}_{\mathbf{zwx}} = \text{cov}(g(\mathbf{x}, \mathbf{z}), g(\mathbf{x}, \mathbf{z})) = \mathbf{K}_{\mathbf{xx}} \odot \left\{ (C_{W|X,Z} \Psi_{\mathbf{x}, \mathbf{z}})^\top (C_{W|X,Z} \Psi_{\mathbf{x}, \mathbf{z}}) \right\}.$$

Combined with the second component, which accounts for the additive noise variance, we have $\mathbf{L}_3 = \mathbf{Q}_{\mathbf{zwx}} + \sigma^2 I$. For \mathbf{L}_2 , we derive a similar inner-product expression for the covariance between $f(x)$ and y :

$$\text{cov}(f(x'), y) = \text{cov}(f(x'), g(x, z)) = k_{x, x'} \langle \mu_W, \mu_{W|X=x, Z=z} \rangle_{\mathcal{H}_W},$$

leading to $\text{cov}(f(\mathbf{x}), \mathbf{y}) = \mathbf{K}_{\mathbf{xx}} \odot (\boldsymbol{\mu}_W)^\top C_{W|X,Z} \Psi_{\mathbf{x}, \mathbf{z}}$. Here, $\boldsymbol{\mu}_W = (\mu_W, \dots, \mu_W)^\top = \mu_W \mathbf{1}_n$ denotes a vector of identical kernel mean embeddings.

Applying Gaussian conditioning yields the following posterior mean and variance expressions:

Proposition 3.6. Let $\tilde{\mathbf{Q}} = (\mathbf{Q}_{\mathbf{zwx}} + \sigma^2 I)$ and $\tilde{\mathbf{C}} = \Psi_{\mathbf{x}} \otimes C_{W|X,Z} \Psi_{\mathbf{x}, \mathbf{z}}$. The posterior $f | \mathcal{D}$ is a GP with mean μ and covariance κ :

$$\begin{aligned} \mu(x) &= (k_x \otimes \mu_W)^\top \tilde{\mathbf{C}} \tilde{\mathbf{Q}}^{-1} \mathbf{y} \\ \kappa(x, x') &= c_W k_{x, x'} - (k_x \otimes \mu_W)^\top \tilde{\mathbf{C}} \tilde{\mathbf{Q}}^{-1} \tilde{\mathbf{C}}^\top (k_{x'} \otimes \mu_W) \end{aligned}$$

We begin by estimating the CMO and the KME of W from the finite sample \mathcal{D} . The CMO is estimated as $\hat{C}_{W|X,Z} = \Psi_{\mathbf{w}}(\mathbf{K}_{\mathbf{xx}} \odot \mathbf{K}_{\mathbf{zz}} + \eta I)^{-1} \Psi_{\mathbf{x},\mathbf{z}}^\top$, which coincides with the first-stage regression in the frequentist kernel regression method [Mastouri et al., 2021, Singh, 2023]. The kernel mean estimator is obtained via the Monte Carlo average $\hat{\mu}_W = n^{-1} \sum_{i=1}^n k_{w_i}$; consequently, the constant appearing in \mathbf{L}_1 is estimated as $\hat{c}_W = n^{-2} \sum_{1 \leq i, j \leq n} k_{w_i, w_j}$. This averaging operation effectively marginalizes W out of the bridge function h . We note that if one instead constructs a joint Gaussian distribution over $h(x, w)$ and $g(x, z)$ and then marginalises W from the posterior of h , the resulting posterior mean for $f | \mathcal{D}$ remains identical.

Therefore, we obtain our empirical estimators for the posterior mean of the structure function,

$$\begin{aligned} \hat{\mu}(x) &= \{\mathbf{K}_{\mathbf{xx}} \odot (\mathbf{K}_{\bar{w}\mathbf{w}} \mathbf{B})\} \{\mathbf{K}_{\mathbf{xx}} \odot (\mathbf{B}^\top \mathbf{K}_{\mathbf{ww}} \mathbf{B}) + \sigma^2 I\}^{-1} \mathbf{y}, \\ \hat{\kappa}(x, x') &= \hat{c}_W k_{x, x'} - \{\mathbf{K}_{\mathbf{xx}} \odot (\mathbf{K}_{\bar{w}\mathbf{w}} \mathbf{B})\} \{\mathbf{K}_{\mathbf{xx}} \odot (\mathbf{B}^\top \mathbf{K}_{\mathbf{ww}} \mathbf{B}) + \sigma^2 I\}^{-1} \{\mathbf{K}_{x'\mathbf{x}} \odot (\mathbf{K}_{\bar{w}\mathbf{w}} \mathbf{B})\}^\top, \end{aligned}$$

where $\mathbf{B} = (\mathbf{K}_{\mathbf{xx}} \odot \mathbf{K}_{\mathbf{zz}} + \eta I)^{-1} (\mathbf{K}_{\mathbf{xx}} \odot \mathbf{K}_{\mathbf{zz}})$ acts as the mediation matrix for proxy setting. Moreover, we denote $\mathbf{K}_{\bar{w}\mathbf{w}} = (\langle \hat{\mu}_W, k_{w_1} \rangle, \dots, \langle \hat{\mu}_W, k_{w_n} \rangle) = \mathbf{K}_{\mathbf{w}\bar{w}}^\top$.

Similarly, we state the relationship between the posterior mean of GPProxy and the frequentist kernel methods:

Proposition 3.7. *Assuming $\mathbf{K}_{\mathbf{xx}} \odot (\mathbf{B}^\top \mathbf{K}_{\mathbf{ww}} \mathbf{B})$ is invertible, the posterior mean of GPProxy is equivalent to the estimator produced by KNC [Singh, 2023].*

However, our operator-based deconditioning method, DProxy, employs a two-stage regression procedure that differs from GPProxy. Specifically, DProxy is equivalent to the original formulation of KNC (version 1) introduced by Singh [2023], which we refer to as KNC-orig. In this version, the first-stage regression involves the conditional mean operator $C_{X,W|X,Z}$, which does not satisfy the completeness assumptions required for identifiability in proximal causal inference [Mastouri et al., 2021]. In contrast, KPV [Mastouri et al., 2021] follows the same regression structure and loss function as GPProxy and KNC, but differs in its representation, leading to a distinct closed-form solution. We refer the reader to Appendix E.2 for further details.

3.3 Hyperparameter Selection

GP models facilitate model selection through marginal log-likelihood optimization [Williams and Rasmussen, 2006]. In our framework, the hyperparameters to be tuned are $\theta_{IV} = (l_x, l_z, \eta, \sigma^2)$ for the IV setting and $\theta_{proxy} = (l_x, l_z, l_w, \eta, \sigma^2)$ for the proxy setting. Here, l_x , l_z , and l_w denote kernel hyperparameters (e.g., length-scale for an RBF kernel), η regularizes the conditional mean operator $C_{X|Z}$, and σ^2 is the noise variance, corresponding to $n\lambda$ in kernel-based second-stage regression methods such as KIV, KPV, and KNE [Singh et al., 2019, Mastouri et al., 2021, Singh, 2023]. By contrast, these kernel-based methods typically fix length-scales using the median heuristic, select other regularization parameters via cross-validation, and employ a data splitting scheme: for instance, in KIV, the data are split into $\mathcal{D}_1 = (\mathbf{x}, \mathbf{y}, \mathbf{z})$ of size m_1 and $\mathcal{D}_2 = (\tilde{\mathbf{x}}, \tilde{\mathbf{y}}, \tilde{\mathbf{z}})$ of size m_2 ; the CME is estimated on \mathcal{D}_1 , and the ATE is then estimated on \mathcal{D}_2 . However, we discourage data splitting, particularly for

small datasets, as it reduces the effective sample size and underutilizes available information. A detailed discussion is provided in Appendix D.

In contrast, our Bayesian GP framework provides a more principled approach to hyperparameter optimization through the marginal likelihood. The log-likelihood of the GP model for IV and proxy is

$$\log p(\mathbf{y}|\theta) \propto -\log |\tilde{\mathbf{Q}}| - \mathbf{y}^T \tilde{\mathbf{Q}}^{-1} \mathbf{y},$$

where $\tilde{\mathbf{Q}}$ denotes $\mathbf{Q}_{zz} + \sigma^2 I$ in the IV setting and $\mathbf{Q}_{zwx} + \sigma^2 I$ in the proxy setting. In practice, we recommend fixing the hyperparameters for z using the median heuristic for l_z and a small value for η (e.g. 0.1), then optimizing all other hyperparameters using the above log-marginal likelihood. This choice is due to identifiability issues regarding the hyperparameters for z (Appendix G.5), and the above scheme drastically improves practical performance. See Appendix G.6 for a sensitivity analysis of this choice.

4 Related Works

IV and Proxy methods. A broad range of methods has been developed for the IV setting. Kernel IV (KIV) [Singh et al., 2019] extend the classical linear two-stage least squares framework by accommodating nonlinear relationships via RKHS representations. To mitigate biases inherent to two-stage procedures, alternative single-stage approaches grounded in the generalized method of moments (GMM) have been proposed, including MMRIV [Zhang et al., 2023], DualIV [Muandet et al., 2019], and its Bayesian counterpart QBIV [Wang et al., 2021]. Deep learning-based IV estimators have also been investigated [Bennett et al., 2019, Xu et al., 2020]. Other Bayesian formulations [Kleibergen and Zivot, 2003, Conley et al., 2008, Lopes and Polson, 2014] have also been studied, but often introduce substantial computational overhead, particularly due to reliance on Markov Chain Monte Carlo (MCMC). More fundamentally, many existing approaches rely on strong and sometimes opaque assumptions about the data-generating process. Although QBIV offers improved scalability, it nevertheless relies on a fictitious data-generating mechanism.

In comparison, methodological developments for proximal causal learning remain relatively limited. Early contributions by Mastouri et al. [2021], Singh [2023] introduced nonlinear estimators based on kernelized two-stage regression, namely KPV and KNC. A GMM formulation tailored to the Proxy setting was also developed in Mastouri et al. [2021]. Subsequently, Wu et al. [2023] proposed doubly robust kernel-based procedures. Deep learning approaches have further extended both two-stage [Xu et al., 2021] and GMM-based [Kompa et al., 2022] paradigms. To the best of our knowledge, the only Bayesian treatment of proximal causal inference is provided by Hu et al. [2023], which employs a probit stick-breaking process prior, whereas our approach instead adopts a Gaussian process prior.

Although several studies in IV and Proxy settings mention UQ, few elaborate on its practical utility or significance. Most existing work evaluates UQ solely through coverage properties, whereas our method further explores applications such as Accuracy-Rejection Curve (learning to reject) [Shaker and Hüllermeier, 2020] and active learning [Aggarwal et al., 2014].

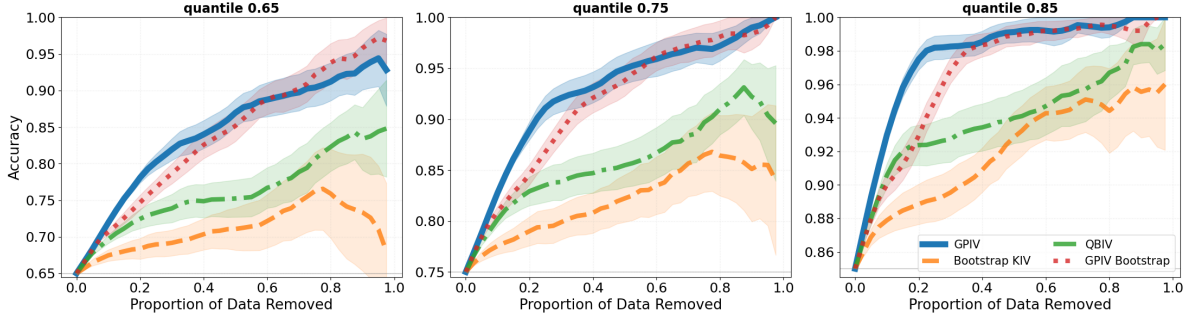


Figure 2: Accuracy-rejection curve for log design (data size = 200), with quantile = 0.65, 0.75, 0.85

Uncertainty quantification (UQ) in causal inference. UQ lies at the core of causal inference, as causal reasoning fundamentally involves counterfactual quantities for which direct observations are typically unavailable — a difficulty known as the fundamental problem of causal inference. Progress on UQ is particularly visible in partially identified settings, where causal estimands cannot be uniquely point-identified [Manski, 2003]. Related work has also relaxed structural assumptions, such as additive noise models in instrumental variable settings, leading to set-based uncertainty characterizations expressed as bounds on the structural function [Kilbertus et al., 2020]. In contrast, our approach maintains the additive structural assumption while adopting a fully probabilistic model to estimate the ATE.

Another prominent line of research focuses on directly quantifying predictive uncertainty in the estimation of causal estimands. GP models have been incorporated into causal inference to enable principled uncertainty quantification, as explored by Chau et al. [2021b], Dimitriou et al. [2024], and Dance et al. [2025]. These approaches typically rely on the assumption of no unobserved confounding, under which uncertainty primarily reflects finite-sample variability and model flexibility. ActiveCQ [Gao and Sejdinovic, 2025] similarly exploits GP posterior uncertainty for active learning, again under the unconfoundedness assumption. In contrast, our work extends this direction to confounded settings by developing GP-based inference procedures for IV and proxy-based identification strategies.

5 Experiments

We evaluate our methods from two dimensions: estimation accuracy and the informativeness of the quantified uncertainty. To assess accuracy, we compare our approach with several widely used baselines, particularly kernel-based methods, using a standard metric: the out-of-sample mean squared error (MSE) between the estimated $\hat{f}(x)$ and the ground-truth ATE function $f(x)$. For uncertainty quantification, besides conventional metrics such as nominal 95% coverage rates [Wang et al., 2021], we also assess the informativeness of the predictive uncertainty using the Accuracy–Rejection Curve (ARC) [Hüllermeier et al., 2022, Chau et al., 2025], which captures the trade-off between prediction accuracy and selective abstention based on uncertainty estimates. ARC visualizes model accuracy as a function of the rejection rate (i.e., the proportion of instances withheld). By selectively abstaining on the $p\%$ of predictions it is least confident about—in our case, those with the highest posterior

variance—the model predicts only on the remaining $(1 - p)\%$ of data. Under informative uncertainty, accuracy improves monotonically with the rejection rate, yielding a rising curve. In contrast, uninformative uncertainty or random abstention results in a flat curve. As existing ARC methods are designed for classification problems, we introduce a continuous analogue termed the δ -ARC. Here, a prediction is considered accurate whenever the absolute error between the predicted and true values falls below a tolerance threshold δ , which is set to certain quantiles of the prediction errors over the test data.

5.1 Simulations on IV

We compare our method, GPIV, against several representative baselines, including KIV [Singh et al., 2019], MMRIV [Zhang et al., 2023], and QBIV [Wang et al., 2021], focusing primarily on estimation accuracy. Notably, KIV differs from GPIV in key design choices, particularly in its reliance on data splitting and the use of fixed kernel lengthscales. QBIV, in contrast, represents a Bayesian extension of DualIV [Muandet et al., 2020]. In the context of UQ, we compare GPIV with QBIV, KIV (BS), and QBIV (BS), where the latter two approaches denote that the initial point estimate is used as the mean estimate, and bootstrap (BS) is employed solely for variance estimation.

Synthetic data. We adopt the data generating process described in Singh et al. [2019], and evaluate each estimator across three distinct designs of the groundtruth ATE f : a sine design ($f(x) = 2 \sin(2\pi x)$), a linear design ($f(x) = 4x - 2$), and a log design ($f(x) = \log(|16x - 8| + 1) \times \text{sgn}(x - 0.5)$) design. To evaluate model performance, we measure the MSE, coverage, and ARC over 200 evenly spaced points $x \in [0, 1]$.

Demand data. We test GPIV on a more challenging airplane ticket demand design used in Muandet et al. [2020]. An observation consists of (Y, P, T, S, C) , where Y, P, T, S, C represents the demand for airline tickets, the price of tickets, the time of year, the sentiment of the customer (discrete variable), and the price shift of the supply cost shifter respectively. Following the notations and methodology in the aforementioned literature, We consider $X = (P, T, S)$ as the input and $Z = (C, T, S)$ as the instruments. The true ATE function is $f(P, T, S) = 100 + S(10 + P)h(T) - 2P$, where $h(T) = 2((T - 5)^4/600 + \exp(-4(T - 5)^2) + T/10 - 2)$. Our test data is the set of 3500 points (p, t, s) , consisting of: 30 evenly spaced values of $p \in [2.5, 27.5]$, 20 evenly spaced values of $t \in [0, 10]$, and all 7 discrete values $s \in \{1, \dots, 7\}$.

Results. Table 1 shows that the proposed method, GPIV, consistently achieves the lowest or second-lowest MSE across all baselines. One contributing factor to the observed performance gap is that KIV requires data splitting, which limits its ability to fully exploit the available samples, whereas GPIV leverages the entire dataset. This effect is evident in the synthetic experiments, where KIV with a sample size of 1000 yields performance comparable to GPIV trained on only 500 samples. We further observe that optimizing the lengthscales associated with X substantially improves accuracy, achieving performance comparable to that of deep learning-based methods [Xu et al., 2020] on the demand design. Additional ablation study on lengthscales and their impact is provided in Appendix G.5.

Table 1: MSE (with standard error in parentheses) for different IV designs and data sizes (n). The best result in each row highlighted in **red** and the second best in **orange**.

Design	n	GPIV	KIV	MMRIV	QBIV
sine	200	.199(.020)	.291(.024)	.199(.015)	.176(.021)
	500	.152(.020)	.224(.024)	.189(.011)	.117(.017)
	1000	.091(.015)	.210(.021)	.160(.008)	.087(.012)
log	200	.142(.019)	.280(.038)	.059(.007)	.177(.022)
	500	.078(.012)	.127(.018)	.058(.005)	.124(.014)
	1000	.045(.008)	.094(.009)	.052(.004)	.090(.011)
linear	200	.165(.020)	.250(.031)	.082(.011)	.193(.024)
	500	.095(.015)	.120(.017)	.093(.008)	.126(.016)
	1000	.057(.009)	.077(.015)	.088(.006)	.069(.007)
demand*	200	.070(.003)	.713(.032)	.649(.025)	.632(.026)
	500	.053(.002)	.605(.030)	.582(.014)	.520(.016)
	1000	.028(.001)	.474(.026)	.539(.013)	.429(.015)

*Note: We report normalized MSE for demand design.

Table 2: Area under quantile 0.75-ARC (the higher the better) and Coverages (the closer to 0.95 the better) with standard error in parentheses, with 200 observations each. The best result in each row is highlighted in **red** and the second best in **orange**.

Design	Metric	GPIV	KIV(BS)	GPIV(BS)	QBIV
sine	AUC	.867(.021)	.790(.022)	.842(.021)	.746(.025)
	Cov.	.900(.082)	.738(.082)	.610(.072)	.876(.137)
log	AUC	.904(.011)	.800(.025)	.893(.012)	.836(.020)
	Cov.	1.00(.000)	.989(.013)	.799(.061)	.746(.159)
linear	AUC	.892(.017)	.832(.024)	.874(.019)	.848(.020)
	Cov.	.993(.011)	.983(.019)	.779(.052)	.771(.162)
demand	AUC	.918(.017)	.663(.008)	.707(.011)	.904(.001)
	Cov.	.961(.007)	.461(.029)	.625(.059)	.903(.010)

We evaluate the quality of the quantified uncertainty using nominal coverage and ARC. Table 2 indicates that GPIV outperforms both the bootstrap-based methods and QBIV in terms of coverage. In particular, the reported 95% confidence intervals of these competing approaches are systematically too narrow, leading to overly optimistic uncertainty estimates. Furthermore, the ARC (Figure 2) and the area under the ARC (AUC in Table 2) indicate that our method provides the most informative uncertainty quantification.

5.2 Simulation on Proxy

We compare our methods GPProxy with several kernel based method: KPV, PMMR [Mastouri et al., 2021], PKIPW, and PKDR [Wu et al., 2023], KNC-orig (equivalent to DProxy) and KNC

Table 3: MSE (with standard error in parentheses) for different data sizes. Superscripts s and d denote synthetic and demand designs, respectively. The best result in each row is highlighted in red and the second best in orange.

n	GProxy	DProxy	PMMR	PKDR	KNC
200 ^s	.385(.041)	.408(.047)	.421(.048)	.401(.032)	.417(.038)
500 ^s	.332(.036)	.374(.030)	.370(.040)	.319(.028)	.372(.029)
1000 ^s	.319(.030)	.354(.035)	.348(.039)	.250(.021)	.390(.030)
200 ^d	16.8(1.80)	19.2(1.47)	18.3(4.03)	14.4(3.40)	18.6(1.32)
500 ^d	13.5(.606)	17.5(.547)	17.1(4.01)	17.3(3.30)	17.7(1.41)
1000 ^d	12.2(.621)	16.1(.551)	15.4(3.93)	15.8(3.36)	16.2(0.43)

Note: KPV and PKIPW are significantly worse than others so their results are not showing here.

Table 4: GProxy vs GProxy(BS):Area under quantile 0.75-ARC and Coverage (Closer to 0.95 the better) across different data size (n) with standard error in parentheses. The best result in each row is highlighted in red.

n	Metric	synthetic		demand	
		GProxy	GProxy(BS)	GProxy	GProxy(BS)
200	AUC	.916(.010)	.842(.018)	.955(.002)	.754(.024)
	Cov	.938(.017)	.803(.026)	.949(.002)	.383(.037)
500	AUC	.934(.004)	.899(.013)	.957(.001)	.713(.036)
	Cov	.929(.014)	.852(.020)	.989(.007)	.389(.024)
1000	AUC	.945(.004)	.922(.007)	.960(.001)	.704(.038)
	Cov	.910(.019)	.772(.024)	.983(.001)	.413(.014)

[Singh, 2023]. For UQ tasks, we compare GProxy with GProxy(BS), which uses variances of bootstrapped posterior means, given that no existing kernel methods in the proximal setting are equipped with uncertainty quantification, to the best of our knowledge.

Synthetic data. We introduce the data generating mechanism for the synthetic experiment. The generative process follows that of Wu et al. [2023]. We choose 300 evenly spaced points for x in $[-2, 4]$ as our test data.

Demand data. We follow the proximal version of the airline demand simulation from Xu et al. [2021] and Kompa et al. [2022]. The objective is to estimate how airline ticket prices X influence sales Y , a relationship confounded by demand U (e.g., seasonal trends). To address this, the fuel cost $Z = (Z_1, Z_2)$ and the number of views on a ticket reservation website W serve as treatment and the outcome proxies, respectively. We evaluate our methods on 300 evenly spaced points for x in $[10, 40]$.

Results. Table 3 shows that our method achieves predictive accuracy comparable to, or exceeding, that of existing kernel-based approaches. Beyond accuracy, our method delivers superior uncertainty quantification relative to bootstrap-based alternatives. This is evidenced by the ARC (Figures 14 and 15) presented in Appendix G.7, where our approach exhibits more informative uncertainty behavior. Consistently, Table 4 demonstrates that our method attains uniformly better coverage across varying sample sizes compared to bootstrap variance estimates.

6 Discussion

We introduced a unified GP framework for IV and Proxy. Leveraging the deconditional perspective, our approach recovers widely used frequentist estimators as posterior means while simultaneously quantifying epistemic uncertainty through the posterior variance. This dual interpretation enables principled model selection via marginal likelihood optimization, contributing to strong predictive performance. Empirical results show that the proposed methods attain competitive accuracy while delivering substantially more informative uncertainty estimates, as reflected in both coverage behavior and selective prediction performance.

Our approach adopts an end-to-end Bayesian framework for inference over the ATE function, where first-stage estimates are treated as parameters defining the likelihood used in the Bayesian update. In principle, it would be desirable to also propagate the predictive uncertainty arising from the first stage. However, incorporating this additional layer of uncertainty would break the closed-form GP structure [Chau et al., 2021b] and necessitate more complex inference and optimization procedures, which lie beyond the scope of this work. We leave this extension for future investigation.

References

- Charu C Aggarwal, Xiangnan Kong, Quanquan Gu, Jiawei Han, and Philip S Yu. Active learning: A survey. In *Data Classification*, pages 599–634. Chapman and Hall/CRC, 2014.
- Virginia Aglietti, Xiaoyu Lu, Andrei Paleyes, and Javier González. Causal bayesian optimization. In *International Conference on Artificial Intelligence and Statistics*, pages 3155–3164. PMLR, 2020.
- Joshua D Angrist and Alan B Krueger. The effect of age at school entry on educational attainment: an application of instrumental variables with moments from two samples. *Journal of the American Statistical Association*, 87(418):328–336, 1992.
- Nachman Aronszajn. Theory of reproducing kernels. *Transactions of the American Mathematical Society*, 68(3):337–404, 1950.
- Andrew Bennett, Nathan Kallus, and Tobias Schnabel. Deep generalized method of moments for instrumental variable analysis. *Advances in Neural Information Processing Systems*, 32, 2019.
- Siu Lun Chau, Shahine Bouabid, and Dino Sejdinovic. Deconditional downscaling with gaussian processes. *Advances in Neural Information Processing Systems*, 34:17813–17825, 2021a.
- Siu Lun Chau, Jean-Francois Ton, Javier González, Yee Teh, and Dino Sejdinovic. Bayesimp: Uncertainty quantification for causal data fusion. *Advances in Neural Information Processing Systems*, 34:3466–3477, 2021b.
- Siu Lun Chau, Michele Caprio, and Krikamol Muandet. Integral imprecise probability metrics. *arXiv preprint arXiv:2505.16156*, 2025.
- Siu Lun Chau, Soroush H Zargarbashi, Yusuf Sale, and Michele Caprio. Quantifying epistemic predictive uncertainty in conformal prediction. *arXiv preprint arXiv:2602.01667*, 2026.
- Zonghao Chen, Atsushi Nitanda, Arthur Gretton, and Taiji Suzuki. Towards a unified analysis of neural networks in nonparametric instrumental variable regression: Optimization and generalization. *arXiv preprint arXiv:2511.14710*, 2025.
- Timothy G Conley, Christian B Hansen, Robert E McCulloch, and Peter E Rossi. A semi-parametric bayesian approach to the instrumental variable problem. *Journal of Econometrics*, 144(1):276–305, 2008.
- Corinna Cortes, Giulia DeSalvo, and Mehryar Mohri. Learning with rejection. In *International Conference on Algorithmic Learning Theory*, pages 67–82. Springer, 2016.
- Hugh Dance, Peter Orbanz, and Arthur Gretton. Interventional processes for causal uncertainty quantification, 2025. URL <https://arxiv.org/abs/2410.14483>.

- Evangelos Dimitriou, Edwin Fong, Karla Diaz-Ordaz, and Brieuc Lehmann. Data fusion for heterogeneous treatment effect estimation with multi-task gaussian processes. *arXiv preprint arXiv:2405.20957*, 2024.
- Yarin Gal, Riashat Islam, and Zoubin Ghahramani. Deep bayesian active learning with image data. In *International Conference on Machine Learning*, pages 1183–1192. PMLR, 2017.
- Erdun Gao and Dino Sejdinovic. Activecq: Active estimation of causal quantities. *arXiv preprint arXiv:2509.24293*, 2025.
- Kelvin Hsu and Fabio Ramos. Bayesian deconditional kernel mean embeddings. In *International Conference on Machine Learning*, pages 2830–2838. PMLR, 2019a.
- Kelvin Hsu and Fabio Ramos. Bayesian Deconditional Kernel Mean Embeddings. In *International Conference on Machine Learning (ICML)*, pages 2830–2838, May 2019b.
- Jie Kate Hu, Dafne Zorzetto, and Francesca Dominici. A bayesian nonparametric method to adjust for unmeasured confounding with negative controls. *arXiv preprint arXiv:2309.02631*, 2023.
- Eyke Hüllermeier, Sébastien Destercke, and Mohammad Hossein Shaker. Quantification of credal uncertainty in machine learning: A critical analysis and empirical comparison. In *Uncertainty in Artificial Intelligence*, pages 548–557. PMLR, 2022.
- Motonobu Kanagawa, Philipp Hennig, Dino Sejdinovic, and Bharath K Sriperumbudur. Gaussian processes and reproducing kernels: Connections and equivalences. *arXiv preprint arXiv:2506.17366*, 2025.
- Niki Kilbertus, Matt J Kusner, and Ricardo Silva. A class of algorithms for general instrumental variable models. *arXiv preprint arXiv:2006.06366*, 2020.
- Ilja Klebanov, Ingmar Schuster, and Timothy John Sullivan. A rigorous theory of conditional mean embeddings. *SIAM Journal on Mathematics of Data Science*, 2(3):583–606, 2020.
- Frank Kleibergen and Eric Zivot. Bayesian and classical approaches to instrumental variable regression. *Journal of Econometrics*, 114(1):29–72, 2003.
- Benjamin Kompa, David Bellamy, Tom Kolokotronis, Andrew Beam, et al. Deep learning methods for proximal inference via maximum moment restriction. *Advances in Neural Information Processing Systems*, 35:11189–11201, 2022.
- Manabu Kuroki and Judea Pearl. Measurement bias and effect restoration in causal inference. *Biometrika*, 101(2):423–437, 2014.
- Marvin Lob, Rahul Singh, and Suhas Vijaykumar. Uniform inference for kernel instrumental variable regression, 2026. URL <https://arxiv.org/abs/2511.21603>.
- Hedibert F Lopes and Nicholas G Polson. Bayesian instrumental variables: priors and likelihoods. *Econometric Reviews*, 33(1-4):100–121, 2014.

- David Madras, Toni Pitassi, and Richard Zemel. Predict responsibly: improving fairness and accuracy by learning to defer. *Advances in Neural Information Processing Systems*, 31, 2018.
- Charles F Manski. *Partial identification of probability distributions*. Springer, 2003.
- Afsaneh Mastouri, Yuchen Zhu, Limor Gultchin, Anna Korba, Ricardo Silva, Matt Kusner, Arthur Gretton, and Krikamol Muandet. Proximal causal learning with kernels: Two-stage estimation and moment restriction. In *International Conference on Machine Learning*, pages 7512–7523. PMLR, 2021.
- Wang Miao, Zhi Geng, and Eric J Tchetgen Tchetgen. Identifying causal effects with proxy variables of an unmeasured confounder. *Biometrika*, 105(4):987–993, 08 2018.
- Wang Miao, Xu Shi, Yilin Li, and Eric J Tchetgen Tchetgen. A confounding bridge approach for double negative control inference on causal effects. *Statistical Theory and Related Fields*, 8(4):262–273, 2024.
- Krikamol Muandet, Bharath Sriperumbudur, Kenji Fukumizu, Arthur Gretton, and Bernhard Schölkopf. Kernel mean shrinkage estimators. *Journal of Machine Learning Research*, 17, 2016.
- Krikamol Muandet, Arash Mehrjou, Si Kai Lee, and Anant Raj. Dual instrumental variable regression. *arXiv preprint arXiv:1910.12358*, 2019.
- Krikamol Muandet, Arash Mehrjou, Si Kai Lee, and Anant Raj. Dual instrumental variable regression. *Advances in Neural Information Processing Systems*, 33:2710–2721, 2020.
- Judea Pearl. *Causality*. Cambridge university press, 2009.
- Carl Edward Rasmussen. Gaussian processes in machine learning. In *Summer school on machine learning*, pages 63–71. Springer, 2003.
- Mohammad Hossein Shaker and Eyke Hüllermeier. Aleatoric and epistemic uncertainty with random forests. In *International Symposium on Intelligent Data Analysis*, pages 444–456. Springer, 2020.
- Rahul Singh. Kernel methods for unobserved confounding: Negative controls, proxies, and instruments, 2023. URL <https://arxiv.org/abs/2012.10315>.
- Rahul Singh, Maneesh Sahani, and Arthur Gretton. Kernel Instrumental Variable Regression. In *Advances in Neural Information Processing Systems*, volume 32. Curran Associates, Inc., 2019.
- Alex Smola, Arthur Gretton, Le Song, and Bernhard Schölkopf. A hilbert space embedding for distributions. In *International Conference on Algorithmic Learning Theory*, pages 13–31. Springer, 2007.

- Le Song, Jonathan Huang, Alex Smola, and Kenji Fukumizu. Hilbert space embeddings of conditional distributions with applications to dynamical systems. In *Proceedings of the 26th Annual International Conference on Machine Learning*, pages 961–968, 2009.
- Le Song, Kenji Fukumizu, and Arthur Gretton. Kernel embeddings of conditional distributions: A unified kernel framework for nonparametric inference in graphical models. *IEEE Signal Processing Magazine*, 30(4):98–111, 2013.
- James H Stock and Francesco Trebbi. Retrospectives: Who invented instrumental variable regression? *Journal of Economic Perspectives*, 17(3):177–194, 2003.
- Eric J Tchetgen Tchetgen, Andrew Ying, Yifan Cui, Xu Shi, and Wang Miao. An introduction to proximal causal learning. *arXiv preprint arXiv:2009.10982*, 2020.
- Kush R Vashney. *Trustworthy machine learning*. Independently published, 2022.
- Ziyu Wang, Yuhao Zhou, Tongzheng Ren, and Jun Zhu. Quasi-bayesian dual instrumental variable regression. *arXiv preprint arXiv:2106.08750*, 2021.
- Christopher K Williams and Carl Edward Rasmussen. *Gaussian processes for machine learning*, volume 2. MIT press Cambridge, MA, 2006.
- Yong Wu, Yanwei Fu, Shouyan Wang, and Xinwei Sun. Doubly robust proximal causal learning for continuous treatments. *arXiv preprint arXiv:2309.12819*, 2023.
- Liyuan Xu, Yutian Chen, Siddarth Srinivasan, Nando de Freitas, Arnaud Doucet, and Arthur Gretton. Learning deep features in instrumental variable regression. *arXiv preprint arXiv:2010.07154*, 2020.
- Liyuan Xu, Heishiro Kanagawa, and Arthur Gretton. Deep proxy causal learning and its application to confounded bandit policy evaluation. *Advances in Neural Information Processing Systems*, 34:26264–26275, 2021.
- Rui Zhang, Masaaki Imaizumi, Bernhard Schölkopf, and Krikamol Muandet. Instrumental variable regression via kernel maximum moment loss. *Journal of Causal Inference*, 11(1):20220073, 2023.

Supplementary Material

A Causal Inference

Here we introduce the omitted assumptions for identifiability in the IV and Proxy setting.

A.1 Instrumental Variable

Assumption A.1. Assumptions to identify the ATE under IV setting:

- *Relevance*: Z has a causal influence on X , i.e., $X \not\perp Z$.
- *Exclusion*: Z does not directly affect Y , i.e., $Y \perp Z \mid (U, X)$.
- *Instrumental Unconfoundedness*: Z is independent of the confounder U , i.e., $U \perp Z$.

A.2 Proximal Causal Learning

Assumption A.2. Assumptions to identify the ATE under Proxy setting [Miao et al., 2018, Mastouri et al., 2021]:

- *Structural Assumptions*: We assume $Y \perp Z \mid (X, U)$, and $W \perp (Z, X) \mid U$
- *Completeness Assumptions*: Let l, g be any square integrable functions, then the following holds:

$$\begin{aligned}\mathbb{E}[l(U) \mid X = x, Z = z] &= 0 \quad \forall (x, z) \in \mathcal{X} \times \mathcal{Z} \iff l(U) = 0 \quad \text{a.s.} \\ \mathbb{E}[g(Z) \mid X = x, W = w] &= 0 \quad \forall (x, w) \in \mathcal{X} \times \mathcal{W} \iff g(Z) = 0 \quad \text{a.s.}\end{aligned}$$

- *Regularity Assumptions*: Please refer to the assumptions (v) - (vii) in the appendix of Miao et al. [2018].

B Deconditioning Operator Methods

Here we introduce the methods using the deconditioning mean operator directly. We begin with the empirical estimator of DMO, provided by [Hsu and Ramos \[2019a\]](#):

$$\hat{D}_{X|Z} = \Psi_{\mathbf{z}}(\mathbf{A}^T \mathbf{K}_{\mathbf{xx}} \mathbf{A} + n\lambda I) \mathbf{A}^T \Psi_{\mathbf{x}}^T, \quad (12)$$

where $\mathbf{A} = (\mathbf{K}_{\mathbf{zz}} + \eta I)^{-1} \mathbf{K}_{\mathbf{zz}}$, and η, λ are the regularization terms for the inversion.

B.1 Deconditioning IV (DIV)

Following the Fredholm integral equation (eq 2), we further represent the conditional expectation $\mathbb{E}[f(X) | Z] = g(Z) = \mathbb{E}[Y | Z]$, for some $g : \mathcal{Z} \rightarrow \mathbf{R}$. We assume $g \in \mathcal{H}_{\mathcal{Z}}$. Using DMO, we may recover the ATE f from the conditional expectation $g: (D_{X|Z})^T g = f$. Hence we have:

$$\begin{aligned} f(x) &= \langle k_x, f \rangle_{\mathcal{H}_{\mathcal{X}}} = \langle k_x, (D_{X|Z})^T g \rangle_{\mathcal{H}_{\mathcal{X}}} \\ &= \langle D_{X|Z} k_x, g \rangle_{\mathcal{H}_{\mathcal{Z}}} \end{aligned}$$

Assume we observe the data \mathcal{D} from the IV structure. Then we express the estimation of f by replacing the DMO with its non-parametric estimator:

$$\hat{f}(x) = \langle \Psi_{\mathbf{z}}(\mathbf{A}^T \mathbf{K}_{\mathbf{xx}} \mathbf{A} + n\lambda I) \mathbf{A}^T \Psi_{\mathbf{x}}^T k_x, g \rangle_{\mathcal{H}_{\mathcal{Z}}} \quad (13)$$

$$= \mathbf{g}^T (\mathbf{A}^T \mathbf{K}_{\mathbf{xx}} \mathbf{A} + n\lambda I) \mathbf{A}^T \Psi_{\mathbf{x}}^T k_x \quad (14)$$

$$= \mathbf{y}^T (\mathbf{A}^T \mathbf{K}_{\mathbf{xx}} \mathbf{A} + n\lambda I) \mathbf{A}^T \mathbf{K}_{\mathbf{xx}} \quad (15)$$

$$= \mathbf{K}_{\mathbf{xx}} \mathbf{A} (\mathbf{A}^T \mathbf{K}_{\mathbf{xx}} \mathbf{A} + n\lambda I) \mathbf{y} \quad (16)$$

where $\mathbf{g} = (g(z_1), \dots, g(z_n)) = \langle \Psi_{\mathbf{z}}, g \rangle_{\mathcal{H}_{\mathcal{Z}}}$. In the second last step, we estimate $g(z_i) = \mathbb{E}[Y | Z = z_i]$ with its point estimate y_i . Denote $\mathbf{y} = (y_1, \dots, y_n)$, then \mathbf{g} is replaced with \mathbf{y} , which follows the same manner in [Hsu and Ramos \[2019a\]](#).

Note that, the last step here can be seen as a kernel regression from Y to Z : $Y = g(Z) + e$, where $g \in \mathcal{H}_{\mathcal{Z}}$ and e is a demeaned error term independent of Z .

B.2 Deconditioning Proxy (DProxy)

Following the similar method in the previous section, we represent $g(X, Z) = \mathbb{E}[Y | X, Z]$ in the (eq 3). The first step is to recover the bridge function h by the DMO

$$h(x, w) = \langle k_x \otimes k_w, (D_{X,W|X,Z})^T g \rangle_{\mathcal{H}_{\mathcal{X}} \times \mathcal{H}_{\mathcal{W}}}. \quad (17)$$

The second step is to integrate U out:

$$\begin{aligned}
f(x) &= \int h(x, W) dP(W) \\
&= \int \langle D_{X,W|X,Z}(k_x \otimes k_W), g \rangle_{\mathcal{H}_X \times \mathcal{H}_Z} dP(W) \\
&= \langle \int D_{X,W|X,Z}(k_x \otimes k_W) dP(W), g \rangle_{\mathcal{H}_X \times \mathcal{H}_Z} \\
&= \langle D_{X,W|X,Z}(k_x \otimes \mu_W), g \rangle_{\mathcal{H}_X \times \mathcal{H}_Z}
\end{aligned}$$

Now we replace the operators with their estimators:

$$\begin{aligned}
\hat{f}(x) &= \langle \hat{D}_{X,W|X,Z}(k_x \otimes \hat{\mu}_W), g \rangle_{\mathcal{H}_X \otimes \mathcal{H}_Z} \\
&= \langle (\Psi_{\mathbf{x}} \otimes \Psi_{\mathbf{z}}) [\mathbf{B}^T (\mathbf{K}_{\mathbf{xx}} \odot \mathbf{K}_{\mathbf{ww}}) \mathbf{B} + n\lambda I]^{-1} \mathbf{B}^T (\Psi_{\mathbf{x}} \otimes \Psi_{\mathbf{w}})^T (k_x \otimes \frac{1}{n} \sum_{i=1}^n k_{w_i}), g \rangle_{\mathcal{H}_X \otimes \mathcal{H}_Z} \\
&= \langle (\Psi_{\mathbf{x}} \otimes \Psi_{\mathbf{z}}), g \rangle_{\mathcal{H}_X \otimes \mathcal{H}_Z} [\mathbf{B}^T (\mathbf{K}_{\mathbf{xx}} \odot \mathbf{K}_{\mathbf{ww}}) \mathbf{B} + n\lambda I]^{-1} \mathbf{B}^T (\mathbf{K}_{\mathbf{xx}} \odot \mathbf{K}_{\mathbf{w}\bar{\mathbf{w}}}) \\
&= (\mathbf{K}_{\mathbf{x}\mathbf{x}} \odot \mathbf{K}_{\bar{\mathbf{w}}\bar{\mathbf{w}}}) \mathbf{B} [\mathbf{B}^T (\mathbf{K}_{\mathbf{xx}} \odot \mathbf{K}_{\mathbf{ww}}) \mathbf{B} + n\lambda I]^{-1} \mathbf{y}
\end{aligned} \tag{18}$$

C Proof and Omitted Assumptions in Section 3

C.1 GP for IV

Assumption C.1. $f \sim \mathcal{GP}(0, k)$ to be integrable: $\int_{\mathcal{X}} |f(X)| dP(X | Z = z) < \infty$

Assumption C.2. The kernel k satisfies

$$\mathbb{E}[[k_X]_{\mathcal{H}_X}] = \int_{\mathcal{X}'} \int_{\mathcal{X}} \sqrt{\text{cov}(f(x), f(x'))} dP(X) dP(X') < \infty.$$

Proposition C.3. (CMP for IV) Under the assumptions (C.1, C.2), the conditional mean process $\{g(z), z \in \mathcal{Z}\}$ induced by f with respect to $P_{X|Z}$ defined as:

$$g(z) = \mathbb{E}_X [f(X) | Z = z] = \int f(X) dP(X | Z = z)$$

is a Gaussian Process $g \sim \mathcal{GP}(0, q)$, with covariance kernel

$$q(z, z') = \text{cov}(g(z), g(z')) = \langle \mu_{X|Z=z}, \mu_{X|Z=z'} \rangle_{\mathcal{H}_X},$$

where $\mu_{X|Z=z}$ denotes the CME of $P_{X|Z=z}$ in the reproducing kernel Hilbert space \mathcal{H}_X .

Proof. The proof consists of two parts.

- CMP, the conditional expectation of a GP remains a valid GP with proper (finite) mean and covariance. This follows the results from [Chau et al. \[2021a\]](#).
- The mean and covariance kernel are 0 and q : We first show the mean of the GP is 0:

$$\mathbb{E}_g[g(z)] = \mathbb{E}_X[\mathbb{E}_f[f(X)] | Z = z] = 0.$$

For covariance kernel, we have,

$$\begin{aligned} q(z, z') &= \text{cov}(g(z), g(z')) \\ &= \iint \text{cov}(f(x), f(x')) dP(X | Z = z) dP(X' | Z = z') \\ &= \mathbb{E}_{X, X'} [k(X, X') | Z = z, Z = z'] \\ &= \langle \mu_{X|Z=z}, \mu_{X|Z=z'} \rangle_{\mathcal{H}_X}, \end{aligned}$$

where the Fubini's theorem is applied to the second step, given the regularity assumption stated in the proposition. □

Covariance Matrices in the joint Gaussian of \mathbf{y} and $f(\mathbf{x})$ in (eq 8) Firstly, we have $\mathbf{M}_1 = \text{cov}(f(\mathbf{x}), f(\mathbf{x})) = \mathbf{K}_{\mathbf{xx}}$ as $\text{cov}(f(x_i), f(x_j)) = k_{x_i, x_j} = [\mathbf{M}_1]_{ij}$

Now, for \mathbf{M}_2 , we have:

$$\begin{aligned}
\text{cov}(f(x), y) &= \text{cov}(f(x), g(z)) \\
&= \int \text{cov}(f(x), f(X)) dP(X | Z = z) \\
&= \int \langle k_x, k_X \rangle_{\mathcal{H}_X} dP(X | Z = z) \\
&= \langle k_x, \int k_X dP(X | Z = z) \rangle_{\mathcal{H}_X} \\
&= \langle k_x, \mu_{X|Z=z} \rangle_{\mathcal{H}_X}.
\end{aligned}$$

Therefore, $\text{cov}(f(\mathbf{x}), \mathbf{y}) = \Psi_{\mathbf{x}}^\top C_{X|Z} \Psi_{\mathbf{z}}$, where

$$C_{X|Z} \Psi_{\mathbf{z}} = [\mu_{X|Z=z_1}, \dots, \mu_{X|Z=z_n}]^\top.$$

For $\mathbf{M}_3 = \mathbf{Q}_{\mathbf{z}\mathbf{z}} + \sigma^2 I$, since we know the additive noise is independent with g , therefore their variance should be additive as well. Therefore we only need to look into the covariance matrix of $g(\mathbf{z})$: $\mathbf{Q}_{\mathbf{z}\mathbf{z}} = (C_{X|Z} \Psi_{\mathbf{z}})^\top (C_{X|Z} \Psi_{\mathbf{z}})$ as

$$\text{cov}(g(z_i), g(z_j)) = \langle \mu_{X|Z=z_i}, \mu_{X|Z=z_j} \rangle_{\mathcal{H}_X} = q(z_i, z_j) = [\mathbf{Q}_{\mathbf{z}\mathbf{z}}]_{i,j}.$$

Therefore, by Gaussian conditioning, we have

$$f(\mathbf{x}) | \mathbf{y} \sim \mathcal{N}(\mathbf{M}_2 \mathbf{M}_3^{-1} \mathbf{y}, \mathbf{M}_1 - \mathbf{M}_2 \mathbf{M}_3^{-1} \mathbf{M}_2^\top). \quad (19)$$

Proposition C.4. Let $\tilde{\mathbf{Q}} = \mathbf{Q}_{\mathbf{z}\mathbf{z}} + \sigma^2 I$. The posterior $f | \mathbf{y}$ given data $(\mathbf{x}, \mathbf{y}, \mathbf{z})$ is a GP with mean μ and covariance κ :

$$\begin{aligned}
\mu(x) &= k_x^\top C_{X|Z} \Psi_{\mathbf{z}} \tilde{\mathbf{Q}}^{-1} \mathbf{y}, \\
\kappa(x, x') &= k_{x,x'} - k_x^\top C_{X|Z} \Psi_{\mathbf{z}} \tilde{\mathbf{Q}}^{-1} \Psi_{\mathbf{z}}^\top C_{X|Z}^\top k_{x'}.
\end{aligned}$$

Proof. Since (eq 19) holds for any \mathbf{x} , by Kolmogorov extension theorem, we have the posterior of f given the observations is a Gaussian Process.

For test points $\tilde{\mathbf{x}} = (x, x')$, $f(\tilde{\mathbf{x}}) | \mathbf{y}$ follows the same expression in (eq 19), so in this case, we have $\mu(x) = [\mathbf{M}_2]_{1,:} \mathbf{M}_3^{-1} \mathbf{y}$, $\kappa(x, x') = [\mathbf{M}_1]_{1,2} - [\mathbf{M}_2]_{1,:} \mathbf{M}_3^{-1} [\mathbf{M}_2]_{:,2}^\top$, where $[\mathbf{M}_1]_{1,2} = k_{x,x'}$ is the covariance between $f(x)$ and $f(x')$, $[\mathbf{M}_2]_{1,:} = k_x^\top C_{X|Z} \Psi_{\mathbf{z}}$, $[\mathbf{M}_2]_{:,2} = k_{x'}^\top C_{X|Z} \Psi_{\mathbf{z}}$ represents the first and second row of the covariance matrix $\text{cov}(f(\tilde{\mathbf{x}}), \mathbf{y})$, where

$$k_x^\top C_{X|Z} \Psi_{\mathbf{z}} = [\langle k_x, \mu_{X|Z=z_1} \rangle_{\mathcal{H}_X}, \dots, \langle k_x, \mu_{X|Z=z_n} \rangle_{\mathcal{H}_X}].$$

$\mathbf{M}_3 = \mathbf{Q}_{\mathbf{z}\mathbf{z}} + \sigma^2 I$ does not change as it only depends on the covariance of \mathbf{y} , which is irrelevant to the new test data points x, x' . \square

C.2 GP for Proxy

Assumption C.5. $P(\cdot|x, z)$ is well-defined for all $(x, z) \in \mathcal{X} \times \mathcal{Z}$.

Assumption C.6. $h \rightarrow \int_{\mathcal{W}} h(x, W) dP(W | X = x, Z = z)$ is a bounded linear functional for every $(x, z) \in \mathcal{X} \times \mathcal{Z}$.

Proposition C.7. (CMP for Proxy) Let $\{g(x, z), x \in \mathcal{X}, z \in \mathcal{Z}\}$ be the CMP induced by the bridge function h

$$g(x, z) = \int_{\mathcal{W}} h(x, W) dP(W|X = x, Z = z).$$

Then, under the assumption of regularity (Assumptions C.5, C.6), by linearity, $g \sim \mathcal{GP}(0, q)$ with the covariance

$$q((x, z), (x', z')) = \text{cov}(g(x, z), g(x', z')) = k_{x, x'} \langle \mu_{W|X=x, Z=z}, \mu_{W|X=x', Z=z'} \rangle_{\mathcal{H}_{\mathcal{W}}}.$$

Proof. The joint Gaussianity is guaranteed as the integration is a linear operation, we refer readers to the proof of Gaussianity to Kanagawa et al. [2025], Section 4. Moreover, we have

$$\mathbb{E}_g[g(x, z)] = \mathbb{E}_h \mathbb{E}_W[h(x, W)|X = x, Z = z] = \mathbb{E}_W[\mathbb{E}_h[h(x, W)]|X = x, Z = z] = 0.$$

For the covariance kernel, we have

$$\begin{aligned} q((x, z), (x', z')) &= \text{cov}(g(x, z), g(x', z')) \\ &= \int \int \text{cov}(h(x, W), h(x', W')) dP(W|X = x, Z = z) dP(W' | X = x', Z = z') \\ &= \int \int k_{x, x'} k_{W, W'} dP(W|X = x, Z = z) dP(W' | X = x', Z = z') \\ &= k_{x, x'} \langle \mu_{W|X=x, Z=z}, \mu_{W|X=x', Z=z'} \rangle_{\mathcal{H}_{\mathcal{W}}}. \end{aligned}$$

□

Assumption C.8. $h \rightarrow \int_{\mathcal{W}} h(x, W) dP(W)$ is a bounded linear functional.

Proposition C.9. Let $f(x) = \int h(x, W) dP(W)$. Under mild regularity assumption C.8, $f \sim \mathcal{GP}(0, r)$ a.s. with the covariance kernel:

$$r(x, x') = \text{cov}(f(x), f(x')) = k_{x, x'} \|\mu_W\|_{\mathcal{H}_{\mathcal{W}}}^2.$$

Proof. Similarly, The joint Gaussianity is guaranteed as the integration is a linear operation [Kanagawa et al., 2025]. Moreover, we have

$$\mathbb{E}_f[f(x)] = \mathbb{E}_h \mathbb{E}_W[h(x, W)] = \mathbb{E}_W[\mathbb{E}_h[h(x, W)]] = 0,$$

and the covariance kernel,

$$\begin{aligned} r(x, x') &= \text{cov}(f(x), f(x')) \\ &= \int_{\mathcal{W}'} \int_{\mathcal{W}} \text{cov}(h(x, W), h(x', W')) dP(W) dP(W') \\ &= \int_{\mathcal{W}'} \int_{\mathcal{W}} k_{x, x'} k_{W, W'} dP(W) dP(W') \\ &= k_{x, x'} \langle \mu_W, \mu_{W'} \rangle_{\mathcal{H}_{\mathcal{W}}} = k_{x, x'} \|\mu_W\|_{\mathcal{H}_{\mathcal{W}}}^2. \end{aligned}$$

Note that, Fubini's theorem is used in the above derivations, which is guaranteed with the regularity assumptions. \square

Covariance Matrices in the Joint Gaussian of \mathbf{y} and $f(\mathbf{x})$ in (eq 11)

$\mathbf{L}_1 = \text{cov}(f(\mathbf{x}), f(\mathbf{x})) = c_W \mathbf{K}_{\mathbf{xx}}$ comes from the covariance kernel r between $f(\mathbf{x})$, where $c_W = \langle \mu_W, \mu_{W'} \rangle_{\mathcal{H}_{\mathcal{W}}} = \|\mu_W\|_{\mathcal{H}_{\mathcal{W}}}^2 = \iint \langle k_W, k_{W'} \rangle dP(W)dP(W')$.

For \mathbf{L}_2 , we have,

$$\begin{aligned} \text{cov}(f(x'), y) &= \text{cov}(f(x'), g(x, z)) \\ &= \text{cov}\left(\int h(x', W') dP(W'), \int h(x, W) dP(W \mid X = x, Z = z)\right) \\ &= \iint \text{cov}(h(x', W'), h(x, W)) dP(W') dP(W \mid X = x, Z = z) \\ &= \iint k_{x, x'} \langle k_{W'}, k_W \rangle dP(W') dP(W \mid X = x, Z = z) \\ &= k_{x, x'} \langle \mu_W, \mu_{W \mid X=x, Z=z} \rangle_{\mathcal{H}_{\mathcal{W}}}. \end{aligned}$$

Note that, we used multiple times of Fubini's theorems in the above derivations. Therefore, we have $\mathbf{L}_2 = \text{cov}(f(\mathbf{x}), \mathbf{y}) = \mathbf{K}_{\mathbf{xx}} \odot (\boldsymbol{\mu}_W)^\top C_{W \mid X, Z} \Psi_{\mathbf{x}, \mathbf{z}}$, where $\boldsymbol{\mu}_W = (\mu_W, \dots, \mu_W)^\top = \mu_W \mathbf{1}_n$, where we again abuse the notation:

$$C_{W \mid X, Z} \Psi_{\mathbf{x}, \mathbf{z}} = [\mu_{W \mid X=x_1, Z=z_1}, \dots, \mu_{W \mid X=x_n, Z=z_n}]^\top.$$

For \mathbf{L}_3 , similar to \mathbf{M}_3 , the covariance consists of the variance of $g(\mathbf{x}, \mathbf{z})$, which is $\mathbf{Q}_{\mathbf{zwx}}$, and the independent additive noise $\sigma^2 I$. The derivation is very similar to the \mathbf{M}_3 and we omitted it here.

Therefore, Gaussian conditioning gives us

$$f(\mathbf{x}) \mid \mathbf{y} \sim \mathcal{N}(\mathbf{L}_2 \mathbf{L}_3^{-1} \mathbf{y}, \mathbf{L}_1 - \mathbf{L}_2 \mathbf{L}_3^{-1} \mathbf{L}_2^\top). \quad (20)$$

Proposition C.10. *Let $\tilde{\mathbf{Q}} = (\mathbf{Q}_{\mathbf{zwx}} + \sigma^2 I)$ and $\tilde{\mathbf{C}} = \Psi_{\mathbf{x}} \otimes C_{W \mid X, Z} \Psi_{\mathbf{x}, \mathbf{z}}$. The posterior $f \mid \mathcal{D}$ is a GP with mean μ and covariance κ :*

$$\begin{aligned} \mu(x) &= (k_x \otimes \mu_W)^\top \tilde{\mathbf{C}} \tilde{\mathbf{Q}}^{-1} \mathbf{y} \\ \kappa(x, x') &= c_W k_{x, x'} - (k_x \otimes \mu_W)^\top \tilde{\mathbf{C}} \tilde{\mathbf{Q}}^{-1} \tilde{\mathbf{C}}^\top (k_{x'} \otimes \mu_W) \end{aligned}$$

Proof. This immediately comes from (eq 20) and the Kolmogorov extension theorem, same as the proof (C.1). \square

D Splitting the Data

Certain methods, particularly two-stage regression approaches [Singh et al., 2019, Mastouri et al., 2021, Singh, 2023], partition the observed data into two distinct sets. For instance, in the instrumental variable setting, one might define $\mathcal{D}_1 = (\mathbf{x}, \mathbf{y}, \mathbf{z})$ and $\mathcal{D}_2 = (\tilde{\mathbf{x}}, \tilde{\mathbf{y}}, \tilde{\mathbf{z}})$. Here, \mathcal{D}_1 is used to train the first-stage model (estimating conditional mean embeddings), while \mathcal{D}_2 is reserved for the second-stage regression. For hyperparameter selection, these methods often minimize the risk associated with one stage using data from the other stage—for example, tuning second-stage hyperparameters based on performance evaluated with \mathcal{D}_1 , and vice versa. In some practical settings, the data may be only partially available across the splits; for instance, \mathcal{D}_1 might contain only (\mathbf{x}, \mathbf{z}) , while \mathcal{D}_2 contains only $(\tilde{\mathbf{y}}, \tilde{\mathbf{z}})$. However, none of these data-splitting scenarios are assumed in our framework. Regarding hyperparameter selection, because lengthscales typically influence both stages of the model, splitting the data and optimizing hyperparameters separately for each stage becomes cumbersome.

In our approach, the first-stage regression (i.e., the estimation of the conditional mean operator) is embedded within the computation of the GP covariance kernel. Consequently, if we were to decouple the estimation of the CMO from the overall procedure, a similar estimation strategy could be applied provided the hyperparameters are fixed. For instance, in the empirical form of the posterior mean and (co-)variance of GPIV, one could replace the mediation matrix $\mathbf{A} = (\mathbf{K}_{\mathbf{z}\mathbf{z}} + \eta I)^{-1} \mathbf{K}_{\mathbf{z}\mathbf{z}}$ with $\tilde{\mathbf{A}} = (\mathbf{K}_{\mathbf{z}\mathbf{z}} + \eta I)^{-1} \mathbf{K}_{\mathbf{z}\tilde{\mathbf{z}}}$, and replace \mathbf{y} with $\tilde{\mathbf{y}}$:

$$\begin{aligned}\hat{\mu}(x) &= \mathbf{K}_{x\mathbf{x}} \tilde{\mathbf{A}} (\tilde{\mathbf{A}}^\top \mathbf{K}_{\mathbf{x}\mathbf{x}} \tilde{\mathbf{A}} + \sigma^2 I)^{-1} \tilde{\mathbf{y}}, \\ \hat{\kappa}(x, x') &= k_{x,x'} - \mathbf{K}_{x\mathbf{x}} \tilde{\mathbf{A}} (\tilde{\mathbf{A}}^\top \mathbf{K}_{\mathbf{x}\mathbf{x}} \tilde{\mathbf{A}} + \sigma^2 I)^{-1} \tilde{\mathbf{A}}^\top \mathbf{K}_{\mathbf{x}x'}.\end{aligned}\tag{21}$$

as our CMO $C_{X|Z}$ is estimated from \mathcal{D}_1 and the remaining GP regression comes from \mathcal{D}_2 .

Similarly, for the proxy setting, our CMO $C_{W|X,Z}$ is estimated from $\mathcal{D}_1 = (\mathbf{x}, \mathbf{y}, \mathbf{z}, \mathbf{w})$ and the remaining GP comes from $\mathcal{D}_2 = (\tilde{\mathbf{x}}, \tilde{\mathbf{y}}, \tilde{\mathbf{z}}, \tilde{\mathbf{w}})$ if we choose to split our data. Therefore, the empirical posterior mean and (co-)variance of GPProxy have the form:

$$\begin{aligned}\hat{\mu}(x) &= \{\mathbf{K}_{x\tilde{\mathbf{x}}} \odot (\mathbf{K}_{\tilde{\mathbf{w}}\tilde{\mathbf{w}}} \tilde{\mathbf{B}})\} \{\mathbf{K}_{\tilde{\mathbf{x}}\tilde{\mathbf{x}}} \odot (\tilde{\mathbf{B}}^\top \mathbf{K}_{\tilde{\mathbf{w}}\tilde{\mathbf{w}}} \tilde{\mathbf{B}}) + \sigma^2 I\}^{-1} \tilde{\mathbf{y}}, \\ \hat{\kappa}(x, x') &= \hat{c}_W k_{x,x'} - \{\mathbf{K}_{x\tilde{\mathbf{x}}} \odot (\mathbf{K}_{\tilde{\mathbf{w}}\tilde{\mathbf{w}}} \tilde{\mathbf{B}})\} \{\mathbf{K}_{\tilde{\mathbf{x}}\tilde{\mathbf{x}}} \odot (\tilde{\mathbf{B}}^\top \mathbf{K}_{\tilde{\mathbf{w}}\tilde{\mathbf{w}}} \tilde{\mathbf{B}}) + \sigma^2 I\}^{-1} \{\mathbf{K}_{x'\tilde{\mathbf{x}}} \odot (\mathbf{K}_{\tilde{\mathbf{w}}\tilde{\mathbf{w}}} \tilde{\mathbf{B}})\}^\top,\end{aligned}\tag{22}$$

where we replace the mediation matrix \mathbf{B} with $\tilde{\mathbf{B}} = (\mathbf{K}_{\mathbf{x}\mathbf{x}} \odot \mathbf{K}_{\mathbf{z}\mathbf{z}} + \eta I)^{-1} (\mathbf{K}_{\mathbf{x}\tilde{\mathbf{x}}} \odot \mathbf{K}_{\mathbf{z}\tilde{\mathbf{z}}})$.

However, we do not recommend doing so, especially when the data size is small. This ensures full use of the available information, which is particularly important when the dataset is limited; splitting the data in such cases would risk underutilizing the already scarce samples. From the synthetic experiments for IV (Table 1), we observe that KIV methods with a training size of 1000 perform similarly to GPIV with a training size of 500. This is largely because data splitting (e.g., an equal split) reduces the effective sample size for each stage, effectively using only half of the information.

E Equivalence Between Methods

E.1 Instrument Variable

Proposition E.1. *(Equivalency between KIV, DIV, and GPIV) Assume that \mathbf{K}_{xx} , $(\mathbf{A}^\top \mathbf{K}_{xx} \mathbf{A} + \sigma^2 I)$ are invertible, the estimator of KIV, DIV, and the mean posterior of GPIV are equivalent.*

Proof. KIV Singh et al. [2019] yields a nonparametric closed-form estimator of f :

$$\hat{f}_{KIV}(x) = (\hat{\alpha})^\top \mathbf{K}_{xx}$$

where $\hat{\alpha} = [\mathbf{K}_{xx} \mathbf{A} (\mathbf{K}_{xx} \mathbf{A})^\top + n\lambda \mathbf{K}_{xx}]^{-1} \mathbf{K}_{xx} \mathbf{A} \mathbf{y}$.

We then derive the following identity:

$$\begin{aligned} \hat{f}_{KIV}(x) &= \mathbf{K}_{xx} [\mathbf{K}_{xx} \mathbf{A} (\mathbf{K}_{xx} \mathbf{A})^\top + n\lambda \mathbf{K}_{xx}]^{-1} \mathbf{K}_{xx} \mathbf{A} \mathbf{y} \\ &= \mathbf{K}_{xx} [\mathbf{K}_{xx} \mathbf{A} \mathbf{A}^\top \mathbf{K}_{xx} + n\lambda \mathbf{K}_{xx}]^{-1} \mathbf{K}_{xx} \mathbf{A} \mathbf{y} \\ &= \mathbf{K}_{xx} [\mathbf{K}_{xx} (\mathbf{A} \mathbf{A}^\top \mathbf{K}_{xx} + n\lambda I)]^{-1} \mathbf{K}_{xx} \mathbf{A} \mathbf{y} \\ &= \mathbf{K}_{xx} (\mathbf{A} \mathbf{A}^\top \mathbf{K}_{xx} + n\lambda I)^{-1} \mathbf{K}_{xx}^{-1} \mathbf{K}_{xx} \mathbf{A} \mathbf{y} \\ &= \mathbf{K}_{xx} (\mathbf{A} \mathbf{A}^\top \mathbf{K}_{xx} + n\lambda I)^{-1} \mathbf{A} \mathbf{y} \\ &= \mathbf{K}_{xx} \mathbf{A} (\mathbf{A}^\top \mathbf{K}_{xx} \mathbf{A} + n\lambda I)^{-1} \mathbf{y} \\ &= \hat{\mu}(x) \end{aligned}$$

where the last step applies the push-through identity—an important corollary of the Woodbury identity.

This closed-form expression coincides with that of Deconditioned IV and with the posterior mean of GPIV, provided the noise variance σ^2 is interpreted as the inverse regularization parameter $n \cdot \lambda$ in the second stage.

Now we only need to prove the equivalency between DIV and GPIV. This is trivial as the estimator in DIV (eq 16) and GPIV (eq 8) are identical. \square

Remark E.2. The equivalence remains valid when the data are split according to the scheme described in Appendix D for both KIV and GPIV, under the assumption that \mathbf{K}_{xx} and $(\tilde{\mathbf{A}}^\top \mathbf{K}_{xx} \tilde{\mathbf{A}} + \sigma^2 I)$ are invertible.

Therefore, the posterior mean of GPIV inherits the good asymptotic behaviors of KIV Singh et al. [2019], Lob et al. [2026].

E.2 Proximal Causal Learning

GPProxy and KNC

Proposition E.3. *Assuming $\mathbf{K}_{xx} \odot (\mathbf{B}^\top \mathbf{K}_{ww} \mathbf{B})$ is invertible, the posterior mean of GPProxy is equivalent to the estimator given by KNC [Singh, 2023].*

Proof. KNC gives a closed-form estimator of bridge function:

$$\hat{h}(x, w) = \{\mathbf{K}_{xx} \odot (\mathbf{K}_{\bar{w}w}\mathbf{B})\}\hat{\alpha},$$

where $\hat{\alpha} = (\mathbf{M}\mathbf{M}^T + n\lambda\mathbf{M})^{-1}\mathbf{M}\mathbf{y}$, $\mathbf{M} = \mathbf{K}_{xx} \odot (\mathbf{B}^\top \mathbf{K}_{ww}\mathbf{B}) = \mathbf{M}^T$, and $\mathbf{B} = (\mathbf{K}_{xx} \odot \mathbf{K}_{zz} + \eta I)^{-1}(\mathbf{K}_{xx} \odot \mathbf{K}_{zz})$ is mediation matrix.

Now we have:

$$\begin{aligned} \hat{\alpha} &= (\mathbf{M}\mathbf{M}^T + n\lambda\mathbf{M})^{-1}\mathbf{M}\mathbf{y} \\ &= \{\mathbf{M}(\mathbf{M}^T + n\lambda I)\}^{-1}\mathbf{M}\mathbf{y} \\ &= (\mathbf{M}^T + n\lambda I)^{-1}\mathbf{M}^{-1}\mathbf{M}\mathbf{y} \\ &= (\mathbf{M}^T + n\lambda I)^{-1}\mathbf{y} \\ &= \{\mathbf{K}_{xx} \odot (\mathbf{B}^\top \mathbf{K}_{ww}\mathbf{B}) + n\lambda I\}^{-1}\mathbf{y}. \end{aligned}$$

Moreover,

$$\begin{aligned} \hat{f}_{KNC}(x) &= \frac{1}{n} \sum_{i=1}^n \hat{h}(x, w_i) \\ &= \frac{1}{n} \sum_{i=1}^n (\mathbf{K}_{xx} \odot \mathbf{K}_{w_i w} \mathbf{B}) \hat{\alpha} \\ &= (\mathbf{K}_{xx} \odot \mathbf{K}_{\bar{w}w} \mathbf{B}) \hat{\alpha}, \end{aligned}$$

which equals to the mean estimator of GPProxy - the noise variance σ^2 is interpreted as the inverse regularization hyperparameter $n \cdot \lambda$ in the second stage regression. \square

Remark E.4. The equivalence remains valid when the data are split according to the scheme described in Appendix D for both KNC and GPProxy, assuming $\mathbf{K}_{\bar{x}\bar{x}} \odot (\tilde{\mathbf{B}}^\top \mathbf{K}_{ww}\tilde{\mathbf{B}})$ is invertible.

Similarly, the posterior mean of GPProxy inherits the asymptotic behaviours from KNC Singh [2023].

KNC and KPV

Both KNC and KPV aim to minimize the empirical loss:

$$\begin{aligned} \hat{\eta}_{XW} &= \operatorname{argmin}_{\eta \in \mathcal{H}_X \times \mathcal{H}_W} \hat{L}(\eta), \text{ where} \\ \hat{L}(\eta) &= \frac{1}{n} \sum_{i=1}^n (y_i - \langle \eta, k_x \otimes \hat{\mu}_{W|x,z} \rangle_{\mathcal{H}_X \times \mathcal{H}_W}) + \lambda \|\eta\|_{\mathcal{H}_X \times \mathcal{H}_W}. \end{aligned}$$

Then, $\hat{f}(x) = \langle \hat{\eta}_{XW}, \hat{\mu}_W \otimes k_x \rangle_{\mathcal{H}_X \times \mathcal{H}_W}$. Both methods use the representer theorem to express $\hat{\eta}_{XW}$ as a linear combination of tensor products of kernel features and CME. However, in KNC, the empirical CME $\hat{\mu}_{W|x,z}$ is first estimated from the first-stage regression, and then $\hat{\eta}_{XW}$ is represented as $\hat{\eta}_{XW} = \sum_{i=1}^n \alpha_i k_{x_i} \otimes \hat{\mu}_{W|x_i, z_i}$, where the coefficients α_i form a vector. In contrast, KPV first expresses $\hat{\mu}_{W|x_i, z_i} = \sum_{j=1}^n \Gamma_j(x_j, z_j) k_{w_j}$, and then represents $\hat{\eta}_{XW}$ as $\hat{\eta}_{XW} = \sum_{i=1}^n \sum_{j=1}^n \alpha_{ij} \Gamma_j(x_j, z_j) k_{x_i} \otimes k_{w_j}$, leading to a matrix of parameters α_{ij} , which differs

from KNC's vector of parameters α_i . This leads to the different closed-form estimator between KPV and KNC (and the posterior mean of GPProxy).

DProxy and KNC-orig

Now, we introduce an alternative kernel regression for the proxy settings, which we named as KNC-orig in our paper. KNC-orig adopts the two stage regression as well, and in the first stage, the operator $C_{X,W|X,Z}$ is obtained from kernel regression. In the second stage, KNC-orig learns the \hat{f} as a mapping from y to $\mu_{X,W|X,Z}$. KPV [Mastouri et al., 2021] and KNC [Singh, 2023], on the other hands, first obtain the operator $C_{W|X,Z}$ and then regress y against $(\mu_{W|x,z}, k_x)$. Mastouri et al. [2021] points out that the first stage of KNC-orig contains self-regression k_x to k_x , which violates the completeness of assumptions, and hence causes bias. Similarly, since $D_{X,W|X,Z}$ contains the CMO $C_{X,W|X,Z}$, it violates the completeness of the assumptions as well.

KNC-orig gives a closed form of the estimator:

$$\begin{aligned} \hat{f}_{KNC-o}(x) &= \frac{1}{n} \sum_{i=1}^n (\mathbf{K}_{xx} \odot \mathbf{K}_{w_i w}) [(\mathbf{K}_{xx} \odot \mathbf{K}_{ww}) \mathbf{B} \mathbf{B}^\top (\mathbf{K}_{xx} \odot \mathbf{K}_{ww}) + n\lambda (\mathbf{K}_{xx} \odot \mathbf{K}_{ww})]^{-1} \\ & (\mathbf{K}_{xx} \odot \mathbf{K}_{ww}) \mathbf{B} \mathbf{y}, \end{aligned} \tag{23}$$

where \mathbf{B} is the mediation matrix.

Corollary E.5. *Under mild invertible assumptions, DProxy and KNC-orig give the same estimator of f .*

Proof. Again, using the Woodbridge identity, we have

$$\begin{aligned} & [(\mathbf{K}_{xx} \odot \mathbf{K}_{ww}) \mathbf{B} \mathbf{B}^\top (\mathbf{K}_{xx} \odot \mathbf{K}_{ww}) + n\lambda (\mathbf{K}_{xx} \odot \mathbf{K}_{ww})]^{-1} (\mathbf{K}_{xx} \odot \mathbf{K}_{ww}) \mathbf{B} \\ &= [\mathbf{B} \mathbf{B}^\top (\mathbf{K}_{xx} \odot \mathbf{K}_{ww}) + n\lambda I]^{-1} \mathbf{B} \\ &= \mathbf{B} [\mathbf{B}^\top (\mathbf{K}_{xx} \odot \mathbf{K}_{ww}) \mathbf{B} + n\lambda I]^{-1} \end{aligned}$$

Rewriting the summation in equation (eq 23):

$$\frac{1}{n} \sum_{i=1}^n (\mathbf{K}_{xx} \odot \mathbf{K}_{w_i w}) = (\mathbf{K}_{xx} \odot \mathbf{K}_{\bar{w}w}),$$

we have

$$\hat{f}_{KNC-o}(x) = (\mathbf{K}_{xx} \odot \mathbf{K}_{\bar{w}w}) \mathbf{B} [\mathbf{B}^\top (\mathbf{K}_{xx} \odot \mathbf{K}_{ww}) \mathbf{B} + n\lambda I]^{-1} \mathbf{y},$$

which is in the same form of DProxy estimator (eq 18). □

F Extension of GPProxy with observed confounders

Some of existing literature [Mastouri et al., 2021, Singh, 2023] also considers scenarios where a subset of the confounders, denoted by C , is observed, as represented in the DAG 3. Under analogous identification assumptions (for details, see Mastouri et al. [2021]), the average treatment effect (ATE) remains identifiable via a Fredholm integral equation of the form:

$$\mathbb{E}[Y | X = x, C = c, Z = z] = \int h(x, c, W) dP(W | X = x, C = c, Z = z).$$

Marginalizing C and W out from the bridge function h , we have the ATE:

$$f(x) = \mathbb{E}[Y | do(X = x)] = \int h(x, c, w) dP(C, W).$$

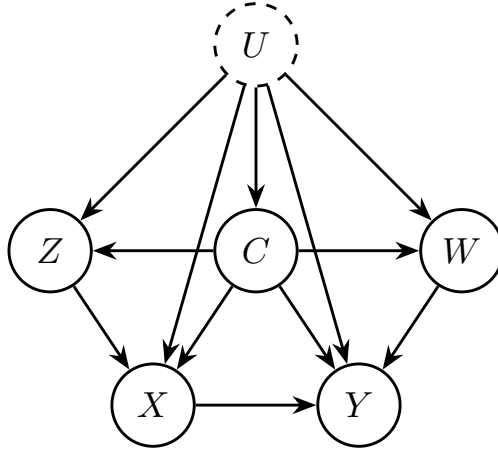


Figure 3: DAG of Proxy setting when the observed confounders exist.

The procedure of construction for the posterior f is similar to the Section 3.2:

- Elicit a GP prior for the bridge function: $h \sim \mathcal{GP}(0, k_X \cdot k_C \cdot k_W)$.
- Let $g(x, c, z) = \mathbb{E}[Y | X = x, C = c, Z = z]$, under regularity assumptions on the covariance kernel, $g \sim \mathcal{GP}(0, q)$ is still a GP under the integration which is a linear operation. Then covariance kernel $q((x, c, z), (x', c', z')) = k_{x,x'} k_{c,c'} \langle \mu_{W|x,c,z}, \mu_{W|x',c',z'} \rangle_{\mathcal{H}_W}$.
- Similarly, $f(x) \sim \mathcal{GP}(0, r)$ under the regularity assumptions, where $r(x, x') = k_{x,x'} \|\mu_W\|_{\mathcal{H}_W}^2$.
- Consider the additive noise model: $\mathbf{y} | \mathbf{x}, \mathbf{c}, \mathbf{z} \sim N(g(\mathbf{x}, \mathbf{c}, \mathbf{z}), \sigma^2 I)$. The properties above guarantees the joint Gaussianity between \mathbf{y} and $f(\mathbf{x})$, where

$$\text{cov}(y, f(x)) = k_{x,x'} \langle \mu_C, k_{c'} \rangle_{\mathcal{H}_C} \langle \mu_W, \mu_{W'|c',x',z'} \rangle_{\mathcal{H}_W}$$

- From Gaussian conditioning, the posterior of f is still a GP with mean $\mu(x)$ and covariance kernel $\kappa(x, x')$:

$$\begin{aligned}\mu(x) &= (k_x \otimes \mu_C \otimes \mu_W)^\top (\Psi_{\mathbf{x}} \otimes \Psi_{\mathbf{c}} \otimes C_{W|C,X,Z} \Psi_{\mathbf{c},\mathbf{x},\mathbf{z}}) (\mathbf{Q} + \sigma^2 I)^{-1} \mathbf{y} \\ \kappa(x, x') &= k_{x,x'} c_{CW} - (k_x \otimes \mu_C \otimes \mu_W)^\top (\Psi_{\mathbf{x}} \otimes \Psi_{\mathbf{c}} \otimes C_{W|C,X,Z} \Psi_{\mathbf{c},\mathbf{x},\mathbf{z}}) (\mathbf{Q} + \sigma^2 I)^{-1} \\ &\quad (\Psi_{\mathbf{x}} \otimes \Psi_{\mathbf{c}} \otimes C_{W|C,X,Z} \Psi_{\mathbf{c},\mathbf{x},\mathbf{z}})^\top (k_{x'} \otimes \mu_C \otimes \mu_W)\end{aligned}$$

where

$$\begin{aligned}\mu_W &= \int k_W dP(W), \\ \mu_C &= \int k_C dP(C), \\ c_{CW} &= \iint \langle \mu_C \otimes \mu_W, \mu_{C'} \otimes \mu_{W'} \rangle_{\mathcal{H}_C \otimes \mathcal{H}_W} dP(C, W) dP(C', W').\end{aligned}$$

Similarly, $\mathbf{Q} = (C_{W|C,X,Z} \Psi_{\mathbf{c},\mathbf{x},\mathbf{z}})^\top (C_{W|C,X,Z} \Psi_{\mathbf{c},\mathbf{x},\mathbf{z}})$.

Substituting the kernel mean embeddings μ_W , μ_C and the operator $C_{W|C,X,Z}$ with their empirical estimators yields the corresponding estimators $\hat{\mu}(x)$ and $\hat{\kappa}(x, x')$.

G Experiments Details and Additional Simulations

G.1 RBF kernel

We use an RBF kernel with amplitude as our GP prior in all of our experiment designs:

$$k(x_1, x_2) = \exp\left(-\frac{(x_1 - x_2)^2}{2l_x^2}\right),$$

where l_x represents the lengthscale.

G.2 IV Experiments Settings

Synthetic data. Here are the details of data generating process:

$$\begin{bmatrix} e \\ V \\ W \end{bmatrix} \sim \mathcal{N}\left(\begin{bmatrix} 0 \\ 0 \\ 0 \end{bmatrix}, \begin{bmatrix} 1 & \rho & 0 \\ \rho & 1 & 0 \\ 0 & 0 & 1 \end{bmatrix}\right)$$

and

$$X = \Phi\left(\frac{W + V}{2}\right), \quad Z = \Phi(W).$$

In the main studies, we set the power of confounding $\rho = 0.5$. Moreover, observations are generated by $Y = f(X) + e$, $E[e|Z] = 0$. Therefore, we have $f(x) = E[Y | do(X = x)]$ which is the average treatment effect (ATE). We test three functions $f(x)$:

1. Sine: $f(x) = 2 \sin(2\pi x)$ (Same as DualIV’s design)
2. Log (Sigmoid): $f(x) = \log(|16x - 8| + 1) \times \text{sgn}(x - 0.5)$ (Same as KIV’s design)
3. Linear: $f(x) = 4x - 2$ (Same as KIV’s design)

We visualize examples for the three designs in figure 4.

We provide the ARC for sine and linear design omitted in the main pages, which shows same behavior across three designs that GPIV perform best across other competitors

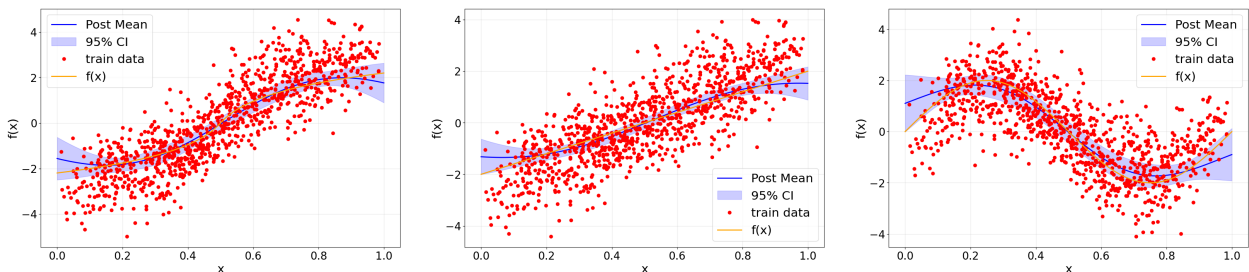


Figure 4: Demo of synthetic data with data size = 1000. Left: log, middle: linear, right:sine.

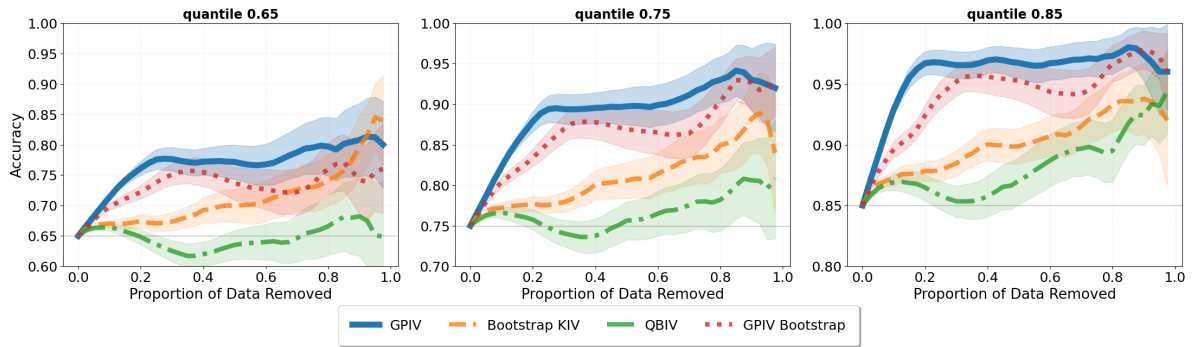


Figure 5: Accuracy-rejection curve for sine design (data size = 200), with quantile = 0.65, 0.75, 0.85.

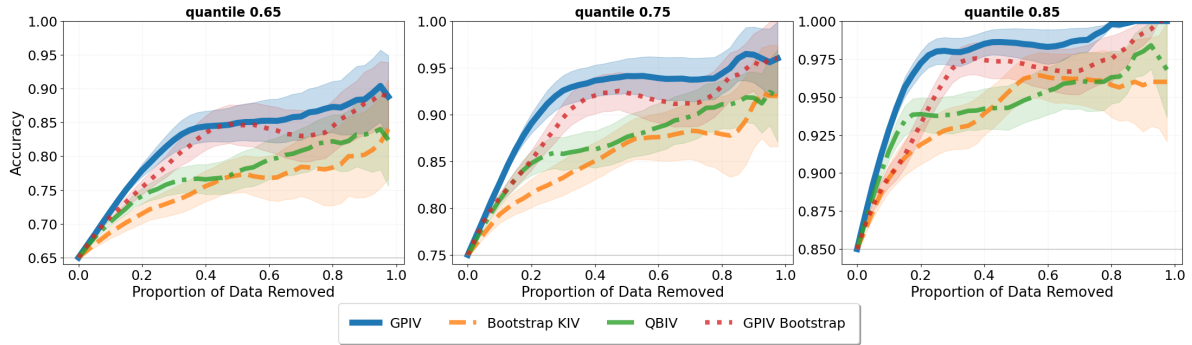


Figure 6: Accuracy-rejection curve for linear design (data size = 200), with quantile = 0.65, 0.75, 0.85.

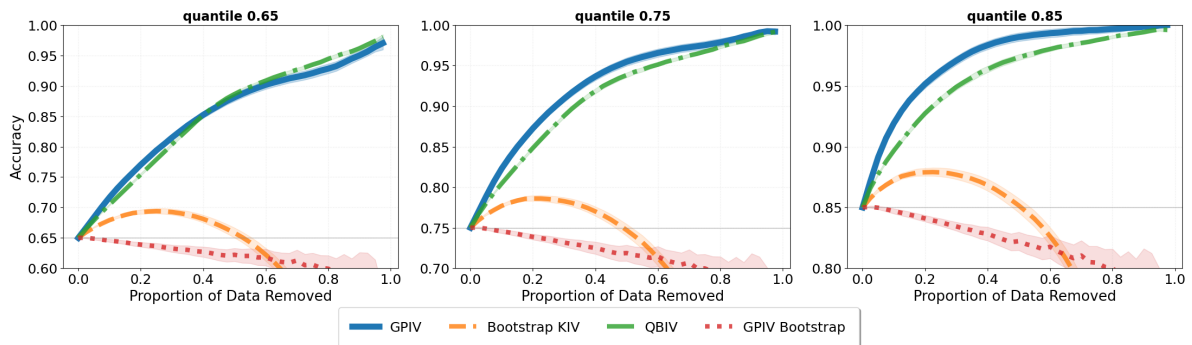


Figure 7: Accuracy-rejection curve for demand design (data size = 200), with quantile = 0.65, 0.75, 0.85.

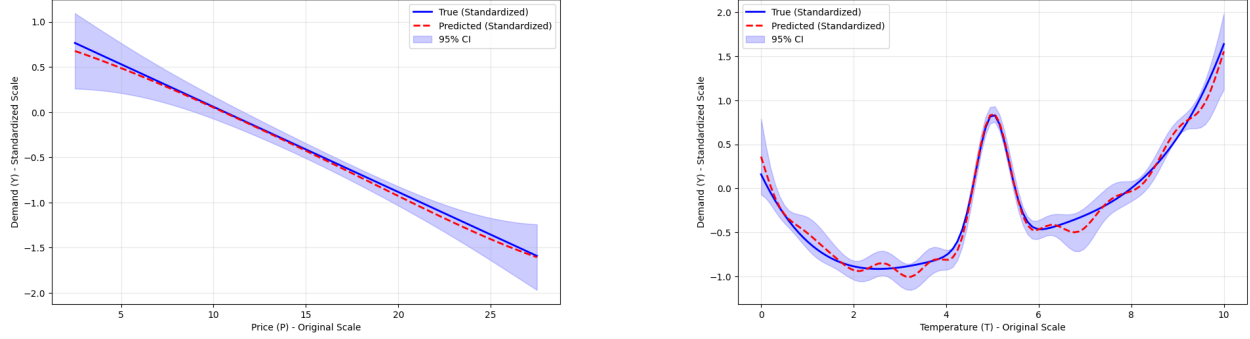


Figure 8: Demo of demand data with data size = 1000. Left: the estimated $\hat{f}(p, t = 2, s = 4)$. Right: the estimated $\hat{f}(p = 20, t, s = 4)$.

Demand data. Data generating process:

$$\begin{aligned}
 S &\sim U\{1, 2, 3, 4, 5, 6, 7\} \\
 T &\sim U[0, 10] \\
 C &\sim N(0, 1) \\
 V &\sim N(0, 1) \\
 \epsilon &\sim N(\rho V, 1 - \rho^2) \\
 P &= 25 + (C + 3)h(T) + V
 \end{aligned}$$

The observation are generated by $Y = f(P, T, S) + \epsilon$, $\mathbb{E}[\epsilon|C, T, S] = 0$. Here we shall consider $X = (P, T, S)$ as the input, and $Z = (C, T, S)$ as the instruments, as the KIV paper suggested.

The structural function is designed as follow:

$$f(P, T, S) = 100 + S(10 + P)f(T) - 2P \quad (24)$$

$$f(T) = 2 \left(\frac{(T - 5)^4}{600} + \exp(-4(T - 5)^2) + \frac{T}{10} - 2 \right) \quad (25)$$

Here we are interested in ATE $f(P, T, S)$, notably, in the DFIV paper, they consider T, S as covariates, P and C as input and instrument variables. Therefore, in their paper, ATE is considered as $f(p) = \mathbb{E}[Y|do(P = p)] = \mathbb{E}_{T,S}[f(p, T, S)]$, and CATE is defined as $\mathbb{E}[Y|do(P = p), T = t] = \mathbb{E}_S[f(p, t, S)]$.

G.3 Ablation Studies on Standard GP and GPIV

When confounding is present, both the posterior mean and variance from a standard Gaussian Process (GP) are affected. Specifically, the posterior mean becomes biased, and the posterior variance is smaller than that of GPIV. This results in an over-confident 95% confidence interval and consequently poor coverage.

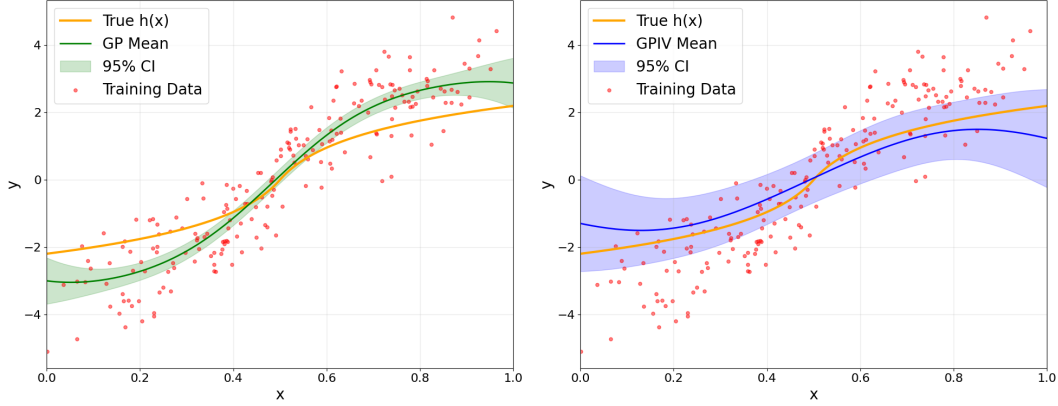


Figure 9: Demo Plots of log design of Standard GP and GPIV with data size = 200

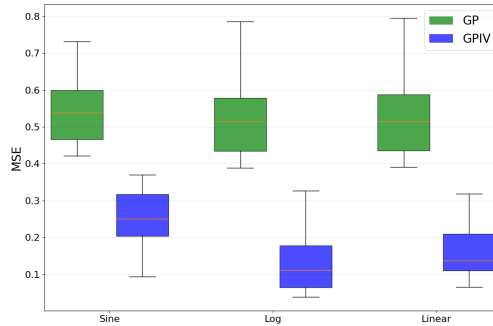


Figure 10: MSE comparison of Standard GP and GPIV.

To illustrate this point, we amplify the confounding effect by increasing the correlation coefficient ρ to 0.9 in the synthetic data generation process.

Figure 9 exemplifies the comparison between the standard GP and GPIV, illustrating that the posterior mean of the standard GP tends to be biased and its posterior variance is underestimated. This leads to an inappropriately narrow confidence interval and consequently inadequate coverage performance.

Figure 10 indicates that bias is consistently observed in the standard GP across all experimental designs due to confounding. Furthermore, the coverage performance of the standard GP is severely compromised, with empirical coverage rates falling between only 13% and 25% across the different designs.

G.4 Additional Studies on Active Learning

We provide an addition study on active learning to test the usefulness and quality of our uncertainty. Active learning [Aggarwal et al., 2014, Gal et al., 2017] is an approach where the model actively selects the most informative data points to be labeled by. Instead of learning from a random, pre-labeled dataset, it asks questions or requests labels for the specific instances it finds most uncertain or valuable. This interactive process allows the model to achieve high accuracy with significantly less labeled data. In causal inference and

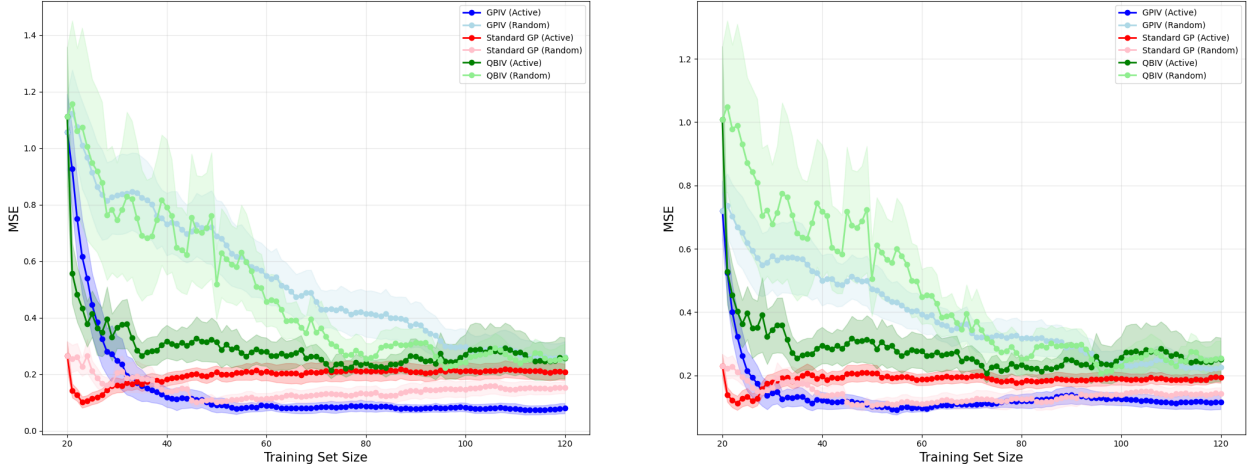


Figure 11: Active Learning of log (left) and linear (right) design.

clinical trial design, labeling patient data or conducting new experiments is often costly. [Gao and Sejdinovic \[2025\]](#) address this by proposing ActiveCQ, an active learning framework for efficiently estimating causal quantities. We test this on our IV setting. Compare with [Gao and Sejdinovic \[2025\]](#), we rank the pooled data by posterior variance and choose the data with the highest posterior variance instead of designed acquisition function:

- Initial Training Data: $\mathcal{D}_T = (x, y, z)_{1:n_T}$, Pooled Data: $\mathcal{D}_P = (\tilde{x}, \tilde{y}, \tilde{z})_{1:n_P}$, and Test data.)
- rank all the pooled data $d \in \mathcal{D}_P$ by their posterior variance, and pick the one with the highest posterior variance, move it to the \mathcal{D}_T . Record the MSE.
- Repeat the previous step until reach the budgets. Plot the MSE against the number of acquired data points.

We set the number of initial training data to be 30, and size of pooled data to be 300. Each time we add one data with the highest variance to the training data, and the budget is 100.

From the figure 11, we show that our method improved faster than our competitors and random learning (randomly adding a new data to the model), which means our posterior mean is informative on choosing the data with the highest potential to improve our model predictions.

G.5 Discussion on the Lengthscales

The ablation study in Table 5 demonstrates that the choice of dimensions for lengthscale optimization significantly impacts model performance on the demand dataset ($n = 200$). Optimizing the lengthscales for dimensions $x = (p, t, s)$ yields the most effective overall results, achieving the lowest MSE, near-nominal coverage probability, and a high AUC. Notably, in both synthetic and demand design settings (both for IV and Proxy), optimizing the lengthscale for z results in an extremely small estimated value, leading to excessively

Table 5: Effect of optimized lengthscales on MSE, Coverage, and Area under AUC with quantile = 0.75 for demand design with 200 data.

lengthscale optimized	MSE	Coverage	AUC
(p, t, s)	.070 (.003)	.961 (.007)	.918 (.003)
(p, t, s, c)	.275 (.030)	.948 (.007)	.923 (.003)
(t, s)	.546 (.020)	.957 (.004)	.931 (.002)
(c, t, s)	.724 (.023)	.930 (.005)	.915 (.002)
\emptyset	.642 (.033)	.851 (.005)	.895 (.002)
(c)	.906 (.043)	.842 (.006)	.866 (.003)
(p)	.206 (.014)	.788 (.006)	.821 (.004)

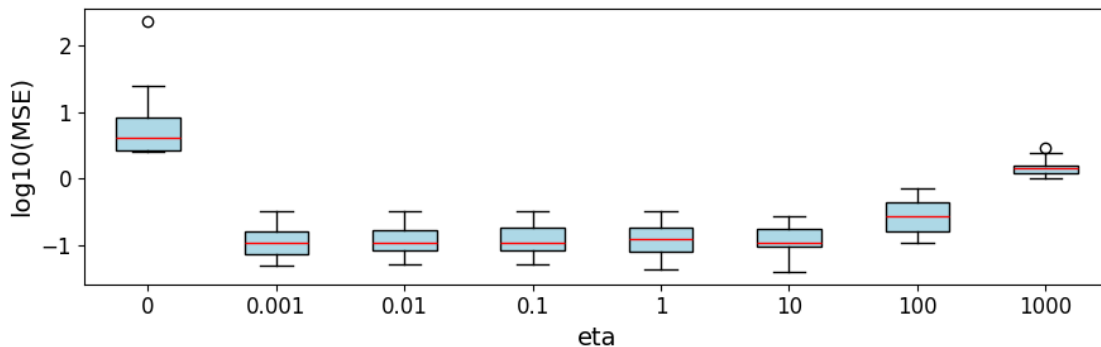


Figure 12: Sensitivity Analysis on η

rough function estimates and consequently poor predictive and uncertainty quantification performance. The results further indicate that optimizing only component c of z —rather than using a median heuristic—produces even worse outcomes.

We observed that, during optimization in both the IV and proxy settings, the lengthscale parameter of Z , denoted as l_z , tends to shrink to very small values (close to zero) across all designs. This lengthscale is highly sensitive to the data, and such instability is detrimental to predictive performance, as an excessively small l_z can lead to overfitting. To address this issue, we recommend fixing l_z using the median heuristic.

G.6 Sensitivity Analysis Study - η

We conduct a sensitivity analysis on the regularization hyperparameter η . We test η over a logarithmic grid ranging from 0.001 to 1000, including $\eta = 0$, using 200 data points. From Figure 12, we observe that the MSE remains quite similar for η values between 0.001 and 1, and deteriorates as regularization increases beyond this range. Moreover, the model also performs poorly when η is very close to or exactly 0. Therefore, we recommend choosing η in the range $[0.01, 1]$, or setting $\eta = 0.001 \cdot n$ if the data are standardized.

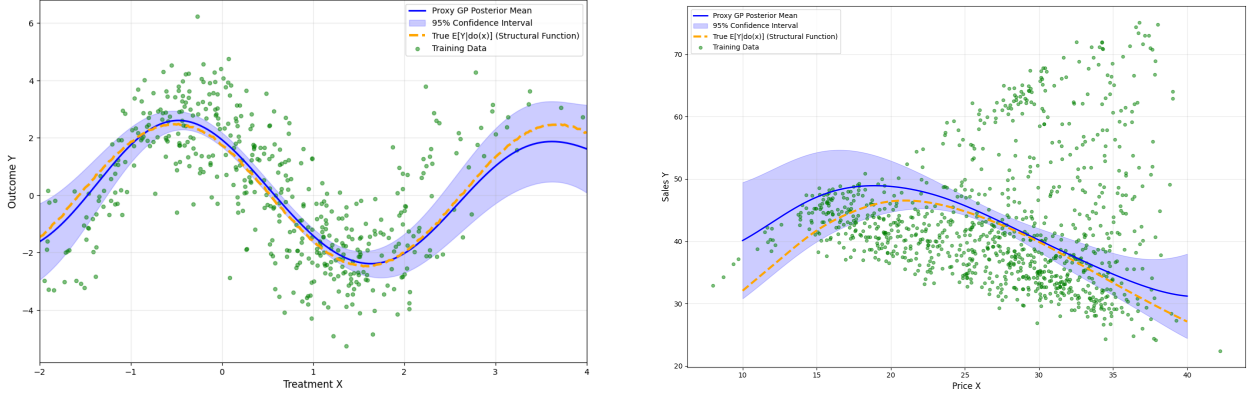


Figure 13: Demo of Proximal synthetic (left) and demand (right) design with 1000 training data.

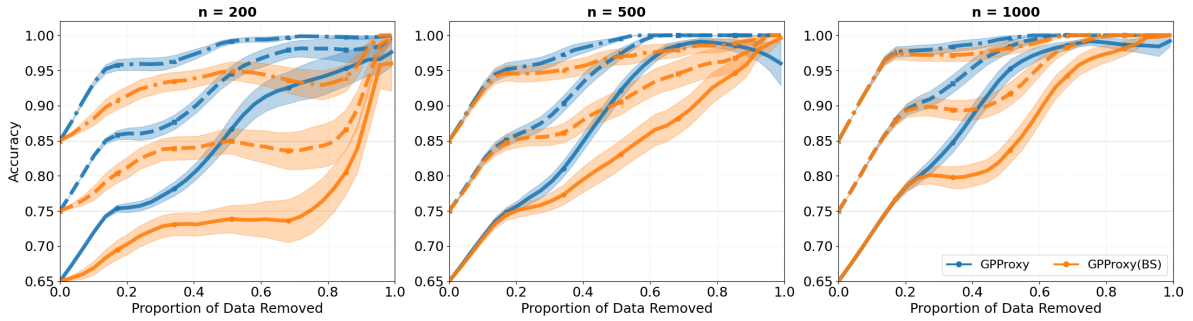


Figure 14: Accuracy-rejection curve for proxy synthetic design (data size = 200, 500, 1000), with quantile = 0.65, 0.75, 0.85.

G.7 Proxy Experiments Settings

Synthetic data. Here are the details of data generating process:

$$\begin{aligned}
 U &:= [U_1, U_2], \quad U_2 \sim \text{Uniform}[-1, 2] \\
 U_1 &\sim \text{Uniform}[0, 1] - \mathbf{1}[0 \leq U_2 \leq 1] \\
 W &:= [W_1, W_2] = [U_1 + \text{Uniform}[-1, 1], U_2 + \varepsilon_1] \\
 Z &:= [Z_1, Z_2] = [U_1 + \varepsilon_2, U_2 + \text{Uniform}[-1, 1]] \\
 X &:= U_2 + \varepsilon_3 \\
 Y &:= 3 \cos(2(0.3U_1 + 0.3U_2 + 0.2) + 1.5A) + \varepsilon_4
 \end{aligned}$$

such that $\varepsilon_{1,2,3,4} \sim N(0, 1)$ independently.

Demand data. Structural equations model real-world pricing with unobserved demand

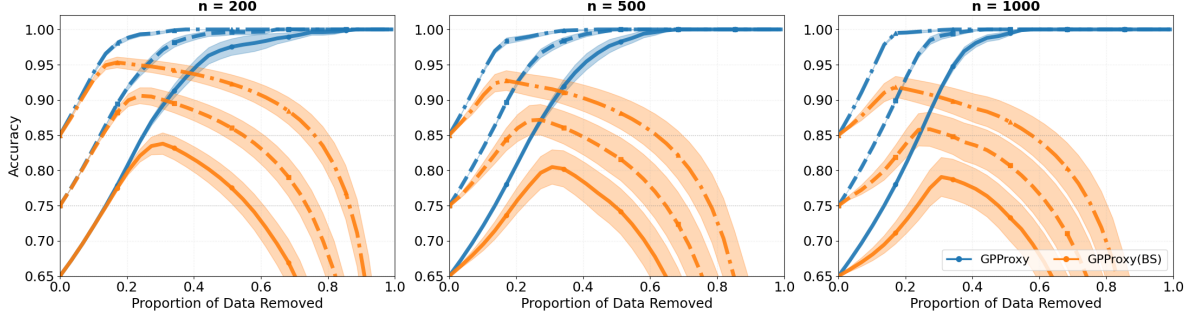


Figure 15: Accuracy-rejection curve for proxy demand design (data size = 200, 500, 1000), with quantile = 0.65, 0.75, 0.85.

sensitivity.

Demand: $U \sim \mathcal{U}(0, 10)$,

Fuel cost: $[Z_1, Z_2] = [2 \sin(2\pi U/10) + \varepsilon_1, 2 \cos(2\pi U/10) + \varepsilon_2]$,

Web views: $W = 7g(U) + 45 + \varepsilon_3$,

Price: $X = 35 + (Z_1 + 3)g(U) + Z_2 + \varepsilon_4$,

Sales: $Y = X \times \min\left(\exp\left(\frac{W - X}{10}\right), 2\right) - 5g(U) + \varepsilon_5$.

where

$$g(u) = 2 \left(\frac{(u-5)^4}{600} + e^{-4(u-5)^2} + \frac{u}{10} - 2 \right), \quad \varepsilon_i \stackrel{\text{i.i.d.}}{\sim} \mathcal{N}(0, 1).$$

Note that we slightly modify the Sales function in Xu et al. [2021] to make the ATE more nonlinear.

G.8 Implementation Details

In practice, jointly optimizing all hyperparameters is not always feasible due to potential nonidentifiability. For both the IV and Proxy settings, we observed that optimizing the lengthscale of Z tends to shrink it to a very small value, leading to extremely poor predictive performance. Therefore, we recommend fixing it using the median heuristic. Moreover, since η serves as a penalization constant, direct optimization via marginal likelihood is not meaningful; we instead set it to a default value of $\eta = 0.1$ in both GPIV and GProxy, as suggested in the section G.6.

We standardize the inputs and optimize the lengthscales of X and W , initializing them with the median heuristic. The noise variance σ^2 is also optimized, with an initial value of 0.25.

In the IV setting, we implement the baseline methods KIV [Singh et al., 2019], MMIV [Zhang et al., 2023], and QBIV [Wang et al., 2021]. For the proximal setting, we include KPV, PMMR [Mastouri et al., 2021], PKIPW, PKDR [Wu et al., 2023], KNC [Singh, 2023],

and KNC-orig (which corresponds to DProxy). For all methods, we adopt the default settings from the original source code: only the regularization hyperparameters are tuned, while the lengthscales are fixed using the median heuristic. Note that the code for KNC and KNC-orig are not publicly available yet; we therefore implement them in Python following the instructions provided in the experimental sections of the respective papers. We re-implement KIV and MMRIV in Python based on their original MATLAB code. In our bootstrap implementation, we used 25 samples per iteration and confirmed that increasing the number of bootstrap iterations does not compromise uncertainty quantification performance. This finding aligns with the conclusions of Wang et al. [2021].

G.9 Wilcoxon Signed-rank test

We employ the Wilcoxon signed-rank test at the 5% significance level to compare the methods. Table 6 lists the methods that perform significantly worse than our approach.

Table 6: Methods with significantly worse performance on MSE than GPIV (left) and GPPProxy (right) under Wilcoxon signed-rank test, 5%.

Design	n	Methods	Design	n	Methods
sine	200	KIV	synthetic	200	–
	500	KIV		500	–
	1000	KIV, MMRIV		1000	–
log	200	KIV	demand	200	–
	500	KIV, QBIV		500	DProxy, KNC
	1000	KIV, MMRIV, QBIV		1000	DProxy, PMMR, PKDR, KNC
linear	200	KIV			
	500	–			
	1000	KIV, MMRIV, QBIV			
demand	200	KIV, MMRIV, QBIV			
	500	KIV, MMRIV, QBIV			
	1000	KIV, MMRIV, QBIV			

Note: For GPIV, the “demand” design uses normalized MSE. “–” indicates no method significantly worse than the our method.